SF 298 MASTER COPY KEEP THIS COPY FOR REPRODUCTION PURPOSES

REPORT DOCUMENTATION PAGE

Form Approved
OMB NO. 0704-0188

1. AGENCY USE ONLY *(Leave blank)*	2. REPORT DATE	3. REPORT TYPE AND DATES COVERED
	11/10/99	Technical Report

4. TITLE AND SUBTITLE

Forced Convection Condensation of Steam Inside a Horizontal Microtube

5. FUNDING NUMBERS

DAAG55-98-1-0205

6. AUTHOR(S)

Shiping Yu
Timothy A. Ameel

7. PERFORMING ORGANIZATION NAME(S) AND ADDRESS(ES)

University of Utah
1471 Federal Way
Salt Lake City, UT 84102-1807

8. PERFORMING ORGANIZATION REPORT NUMBER

9. SPONSORING / MONITORING AGENCY NAME(S) AND ADDRESS(ES)

U.S. ARMY RESEARCH OFFICE
P.O. BOX 12211
RESEARCH TRIANGLE PARK, NC 27709-2211

10. SPONSORING / MONITORING AGENCY REPORT NUMBER

ARO 38757.1-PH

11. SUPPLEMENTARY NOTES

The views, opinions and/or findings contained in this report are those of the author(s) and should not be construed as an official Department of the Army position, policy, or decision, unless so designated by other documentation.

12a. DISTRIBUTION / AVAILABILITY STATEMENT

Approved for public release; distribution unlimited.

12b. DISTRIBUTION CODE

19991215 027

13. ABSTRACT *(Maximum 200 words)*

Preliminary experimental results of forced convection condensation of steam inside a horizontal microtube are reported. The stainless steel microtube has a diameter of 250 μm and a length of 48 mm. The inlet saturated vapor Reynolds number ranges from 390 to 4,700 and the average inlet saturated vapor velocities range from 33 to 276 m/s. The mean subcooled temperature varies from 12 to 25°C. The two-phase pressure drop ranges from near zero to 65 kPa. The vapor quality at the inlet and outlet are 100% and 24 to 94%, respectively. The experimental average Nusselt numbers are compared to those from stratified condensation flow and annular condensation flow in macrotubes found in the literature. The experimental average Nusselt numbers are (1) 3 to 50 times smaller than the macrotube values, (2) do not depend on the inlet saturated vapor Reynolds number or velocity, and (3) increase nearly linearly with the increase in the change of vapor quality from the inlet to the outlet. The significant deviation from macroscale theory observed may be due to different condensation mechanisms caused by the relatively large droplet sizes relative to the inside diameter of the microtube. The two-phase pressure drop should include the contribution of surface tension.

14. SUBJECT TERMS

This document describes experiments performed to assess condensation heat transfer in cylindrical microtubes. The tubes are the smallest ever used in a condensation experiment.

15. NUMBER OF PAGES

67

16. PRICE CODE

17. SECURITY CLASSIFICATION OR REPORT	18. SECURITY CLASSIFICATION OF THIS PAGE	19. SECURITY CLASSIFICATION OF ABSTRACT	20. LIMITATION OF ABSTRACT
UNCLASSIFIED	UNCLASSIFIED	UNCLASSIFIED	UL

THE UNIVERSITY OF UTAH

Technical Report: Forced Convection Condensation of Steam Inside a Horizontal Microtube

by
Shiping Yu and Tim Ameel

Department of Mechanical Engineering
50 S. Central Campus Drive, MEB 2202
University of Utah
Salt Lake City, UT 84112

In Partial Fulfillment of
Grant Number DAAG55-98-1-0205
"Condensation in Microchannels"
PI: Tim Ameel, University of Utah

U.S. Army Research Office
4300 South Miami Blvd.
P.O. Box 12211
Research Triangle Park, North Carolina 27709-2211

November, 1999

ABSTRACT

This thesis reports preliminary experimental results of forced convection condensation of steam inside a horizontal microtube. The stainless steel microtube has a diameter of $250\mu m$ and a length of $48mm$. The inlet saturated vapor Reynolds numbers range from 390 to 4,700, and the average inlet saturated vapor velocities are from 33 to $276m/s$. Dimensionless vapor velocities (ratio of vapor shear axial gradient to gravity radial gradient) are from 15 to 150, and liquid volumetric fraction in the vapor is from 2.3×10^{-4} to 41×10^{-4}. The mean subcooled temperature varies from 12 to 25°C. Two phase pressure drops range from near zero to $65kPa$. The vapor quality at the inlet and outlet is 100% and $24 \sim 94\%$, respectively. The experimental average Nusselt numbers are compared to those from the stratified condensation flow and annular condensation flow in macrotubes found in the literature. It is found that the experimental average Nusselt numbers (1) are 3 to 50 times smaller than the macrotube results, (2) do not depend on the inlet saturated vapor Reynolds numbers or inlet saturated vapor velocities, and (3) increase nearly linearly with the increase in the change of vapor quality from the inlet to outlet. The significant deviations from macroscale theory observed may be due to a different condensation mechanism caused by relatively large droplet sizes compared to the inside diameter of the microtube. The two-phase pressure drop should include the contribution of surface tension.

CONTENTS

LIST OF TABLES

LIST OF FIGURES

NOMENCLATURE

A_0	cross-sectional area of the microtube
A_1	cross-sectional area of the tubing that connects the inlet of the microtube
C	coefficient, Eq. (2.26)
c_p	specific heat at constant pressure
d	diameter
D	diameter of the tubing that connects the inlet of the microtube
D_{10}	average linear diameter of droplet, defined in [43]
f	friction factor
F	wall shear stress/function
g	acceleration of gravity
G	mass flow velocity, $\dot{m}/A_0$
h	heat transfer coefficient/enthalpy
j_G^*	dimensionless vapor velocity
k	thermal conductivity
K_c	contraction coefficient of flow
K_e	compression coefficient of flow
L	length of the microtube
m	exponent, Eq. (2.26)
$\dot{m}$	mass flowrate
n	exponent, Eq. (2.26)
Nu	Nusselt number
p_r	reduced pressure
P	pressure
Pr	Prandtl number
ΔP	pressure drop
$\dot{q}$	heat flux
$\dot{Q}$	rate of heat transfer
Re	Reynolds number
T	temperature
ΔT	subcooled temperature difference
ΔT^*	dimensionless temperature
u	velocity
v	specific volume
$\dot{V}$	volumetric flowrate
x	vapor quality/variables in uncertainty analysis

X Eq. (2.26)
α void fraction
β constant relating interfacial liquid velocity to the average velocity throughout the condensate film, Eq. (2.13)
δ thickness of wall/delta in uncertainty analysis
ϵ incremental variables in uncertainty analysis
μ viscosity
ρ density
σ surface tension
ϕ multiplier, Eq.(2.24) and Eq. (2.25)

Superscript

- mean

Subscript

1 inlet
2 outlet
cd condensation
eq equivalent
f liquid/friction
fg saturated mixture of two phase
g gas
i inlet/inside
m mean/momentum
o outlet/outside
sat saturated
$spht$ superheated
t total
w water
wl wall
σ surface tension

ACKNOWLEDGEMENTS

I am very grateful to my advisor Dr. Tim A. Ameel for his excellent guidance and patience in this research.

My sincere thanks extend to Dr. A. Bruno Frazier and Dr. Patrick A. McMurtry for being on the thesis committee and for their interest and comments.

I would like to thank my wife, Yan He, for her continued moral and emotional support. I wish to express my gratitude to my parents for their endless love and encouragement throughout my entire education.

CHAPTER 1

INTRODUCTION

In the past decade there has developed a growing interest in microscale systems and devices, or microelectromechanical systems (MEMS) technology. Potential applications of MEMS technology may be found in fields such as bioengineering and biotechnology, aerospace, mini heaters and electronic cooling heatsinks and heat exchangers, electronics and microelectronics, material processing, thin film deposition technology, micro optics, micro sensors and processors, micro heat pumps and heat pipes, and micro vapor compression refrigeration systems. Past work on MEMS technology has primarily been directed toward fabrication techniques and considerable progress has been made in this area. As a consequence, emphasis in MEMS technology is beginning to include the analysis and design of micro systems. Better understanding of microscale flow and heat transfer will help to assess the combined influences of mechanical, electromagnetic, thermal, optical, and fluid properties and processes [1, 2, 3].

Two general areas of research concerning microscale flow and heat transfer are being studied. One is single-phase flow and heat transfer, and the second concerns two-phase flow and heat transfer with/without phase change. To date, however, work in investigating two-phase condensation in microchannels or microtubes has not been found. If the main task in the previous study of microscale two-phase flow boiling and heat transfer has been directed toward removing heat from high heat flux components (microelectronic chips, LSICs, laser devices, etc.), it was understandable why microscale two-phase condensation has not yet been dealt with. The importance of understanding the mechanisms and fundamental differences involved with flow and heat transfer in two phase condensation in microgeometries

can be seen in some promising applications including the design of industrial mini condensers, the construction of micro vapor power systems and micro vapor compression refrigeration systems, and the design of micro heat pipes, etc. Therefore, it is the lack of the work in this area and the potential microscale applications that provoke the interest of the current research.

1.1 Review of Microscale Flow and Heat Transfer

General strategies used for MEMS technology are to microfabricate individual components of a large-scale system in order to improve the system, and/or to design and build a completely new microscale device with functionality comparable to a macroscale system. However, the downsizing of components or systems may result in some special effects. The scaling effects are one of the most important factors to be assessed in the design process [4]. For example, the linear increase in surface-area-to-volume ratio with scale reduction of an energy conversion and transport system will improve surface processes such as convection heat transfer and adsorption [4]. The scaling effect in convection heat transfer can be shown by an example of internal convection. In laminar fully-developed flow (most microtube flow is laminar) with characteristic dimension d, the heat flux scales as d^{-1} while the pressure drop scales as d^{-4} for constant mass flow rate. Thus, the heat transfer is much less sensitive to scale than the pressure drop. Scaling effects for external convection, radiation, and phase change processes are more complicated.

Sizes of MEMS components or systems range from micrometers to millimeters. At these scales, in addition to the scaling effects mentioned above, actual processes associated with fluid flow and heat transfer in microgeometries may deal with a number of other microscale factors such as viscosity variation near the surfaces, slip flow at the boundaries, compressibility, and microcontinuum effects [5]. For example, it has been shown that for gas flow in very small channels the continuum assumptions may break down when the molecular mean free path is on the order of the dimensions of the channel [6, 7, 8]. Other observed microscale effects included two- and three- dimensional transport effects [9], and effects of temperature

variations of the transport fluid [10].

By far, the majority of the reported research in microscale flow and heat transfer is based on empirical or semiempirical correlations of experimental results and no universally accepted theoretical models are available.

Single-phase flow and heat transfer in microgeometries has been the most extensively investigated field. This research was initiated by the work of Tuckerman [11] who used microchannels of about $50\mu m$ to cool micro electronic chips. A $790W/cm^2$ heat flux was removed from the silicon chips using water with a pressure drop of about 2 atm and a $71°C$ temperature rise above the fluid. Since then, a considerable number of related research projects have been conducted. Phillips [12] developed a complete resistance model to predict heat transfer and flow performance of microchannels by improving on the Tuckerman model [11]. Weisberg et al. [13] conducted a numerical analysis of heat transfer in a microchannel and acquired the profile of the Nusselt number along the walls of the microchannel. Yu et al. [14] developed a simple resistance model to design an air-cooled microchannel heatsink used for the cooling of a high power Traveling Wave Tube (TWT). In addition to theoretical investigations, several small scale devices or systems that make use of single-phase convection have been developed. Examples include small scale silicon thermal flow sensors [15], microscale pressure sensors [16], micromembane pumps [17], cooling devices for carbon dioxide laser arrays [18], a mini heatsink for a high power TWT [14], etc. A maximum heat flux of $1300W/cm^2$ for water cooling has been reported by Koh et al. [19]. Recently, Yu at al. [14] reported an air-cooled microchannel mini heatsink that was used to remove a heat flux of up to $14W/cm^2$ from a high power TWT with the characteristic of low pressure drop. However, the models used for the above investigations are mostly based on macroscale assumptions. For instance, the Nusselt number in the microchannel usually takes on a value that is from that acquired between two macroscale infinite parallel flat plates with an isoflux boundary condition when the aspect ratio of the microchannel is large enough [19, 12, 14, 20]. Such a treatment would undoubtedly offer a means to realize preliminary engineering applications, but it may have

obscured possible microscale effects due to the approximations used in the models [14, 20]. Although a large number of studies have been directed toward detecting microscale effects for single phase flow and heat transfer, the current research seems not to be able to reach conclusive results due to the insufficiency of data and inconsistence between experiments. General conclusions that may be made on the microscale effects in single phase flow and heat transfer include [1]: (1) friction factors in laminar microchannel flow are apparently lower than macroscale predictions at the same Re, (2) turbulent heat transfer coefficients are apparently higher than theory predicts at the same Re, (3) microscale effects seem to become more prominent for channels smaller than $40\mu m$, (4) slip flow theories appears to be applicable to only the smallest channels in gas flow, and (5) based on (1) and (2), the Reynolds analogy appears to be invalid in the microscale regime.

Two-phase flow and heat transfer with/without phase change is another type on microchannel process important for the development of complete systems. The major advantage of two-phase heat transfer with phase change is that the temperature gradient along the length of flow is much smaller than in single-phase flow. This results in larger values of the heat transfer coefficient and reduces the requirement of large flow rates. Research of boiling heat transfer in open and closed microchannels has achieved some significant results. The minimum channel size for which data are available is approximately $100\mu m$. Maximum heat fluxes of $350W/cm^2$, $130W/cm^2$, and $80W/cm^2$ have been found for open and closed microchannel convection flow boiling, and micro heat pipes, respectively [3]. The magnitude of these heat flux data indicate why two-phase heat transfer is such an important area of research. Some of the most promising areas for future development are the areas of liquid metal heat pipes and micro vapor compression cycles. Convective flow boiling in microgeometries appears to be a technology that can satisfy the demand for the dissipation of high heat fluxes associated with electronic and laser devices. However, at this time, the amount of work available in the literature related to open and closed microchannels is quite limited. Some progress concerning convective flow boiling in microgeometries has been made by the work of Zhukov and Yarmak [21],

that of Peng and Wang [2], and that of Bowers and Mudawar [22]. Although some obvious differences of performance compared to that in macrogeometries have been observed in their work, no general conclusions can be drawn in this area.

Presently, the area of microscale two phase flow and heat transfer without phase change is being dealt with. The only work found in this area is that of Suo and Griffith [23], and that of Stanley [24] .

1.2 Objectives of Current Research

As mentioned earlier, work in microscale condensation flow and heat transfer has not been seen in the literature. As a result, the current research should be expected to shed considerable light on this field. The goal of this research is to experimentally investigate condensation flow and heat transfer of steam forced convection in a horizontal microtube. A stainless steel microtube with inside diameter of 250μm will be used for the research. The experiments will be expected to determine condensation Nusselt numbers and condensation pressure drops in the range of Reynolds numbers of inlet saturated vapor approximately from 500 to 5,000. This selected range of Reynolds numbers is due to the consideration that the resulting pressure drops would be appropriate for actual applications. Experimental outcomes will be compared to macroscale results available in the literature to identify possible microscale effects.

CHAPTER 2

REVIEW OF MACROSCALE CONDENSATION

As mentioned in Chapter 1, there have not been any experiments reported in the literature for condensation flow and heat transfer in microgeometries. This chapter will review some widely used and accepted results acquired for macroscale condensation, which will be used for comparison with the current experiment. Types of condensation will first be introduced, and then correlations for condensation heat transfer and the method to obtain condensation pressure drop will be described.

2.1 Types of Condensation

Condensation is one of the most common modes of heat transfer. Condensation is defined as the removal of heat from a system in such a manner that vapor is converted into liquid. There are various ways in which condensate may be formed. The different mechanisms are known as the modes of condensation. The major modes include dropwise condensation and film condensation. Since it is impossible to maintain cooling surfaces in a state that maintains dropwise condensation for long periods of time, film condensation is of practical importance in applications for industrial condensers. In this mode, the condensate wets the surface and forms a continuous liquid film.

Film condensation can occur on an outside surface or on an inside surface of a tube. For the latter form, film condensation takes place when the flowing vapor is driven through the subcooled inside surface of the tube. Depending on the orientation of the tube, this flowing condensation can be divided into horizontal, vertical, and inclined condensation in the tube. Film condensation inside horizontal tubes will be of interest in the current research.

2.2 Pattern Identification of Film Condensation

Flow patterns of film condensation inside a horizontal tube depend on the distribution of forces in the fluid and the amount of condensate in a cross section. These flow patterns are shown in Figure 2.1 [25].

If the vapor shear stress on the condensate film is sufficiently large in comparison to the effect of gravity, and if the amount of condensate is small, then there will be an annular flow.

If the velocity of the vapor flow is moderate, the influence of gravity will cause the condensate to flow off around the circumference of the wall, which results in a condensation pattern called stratified flow.

Spray flow is the result of shear of high velocity vapor. In this pattern, a small amount of liquid from the inside surface of the tube is entrained into the core of the tube and forms a smog mixture of vapor and liquid.

Other flow patterns include intermittent flow and bubble flow. An intermittent flow, which consist of liquid with trapped vapor bubbles or of a liquid slug with vapor zones extending to the wall, forms a low vapor velocity but with a large liquid component. At a high vapor velocity and in a large liquid component, a bubble flow with bubbles being distributed in a cohesive liquid, will result.

For the calculation of heat transfer, one must first estimate which flow pattern is present. A starting point for this is to use the flow pattern chart shown in Figure 2.1. In this chart, the term $(1-\alpha)/\alpha$ in the horizontal axis represents liquid volumetric fraction where α is void fraction of the vapor which is related to vapor quality as

$$\alpha = \left[1 + \frac{1-x}{x}\left(\frac{\rho_g}{\rho_f}\right)^{2/3}\right]^{-1}, \tag{2.1}$$

and j_G^* in the vertical axis is the dimensionless vapor velocity, which is the ratio of vapor shear axial gradient to gravity radial gradient, that is

$$j_G^* = \frac{x\dot{m}}{A_0[gd_i\rho_g(\rho_f - \rho_g)]^{1/2}}. \tag{2.2}$$

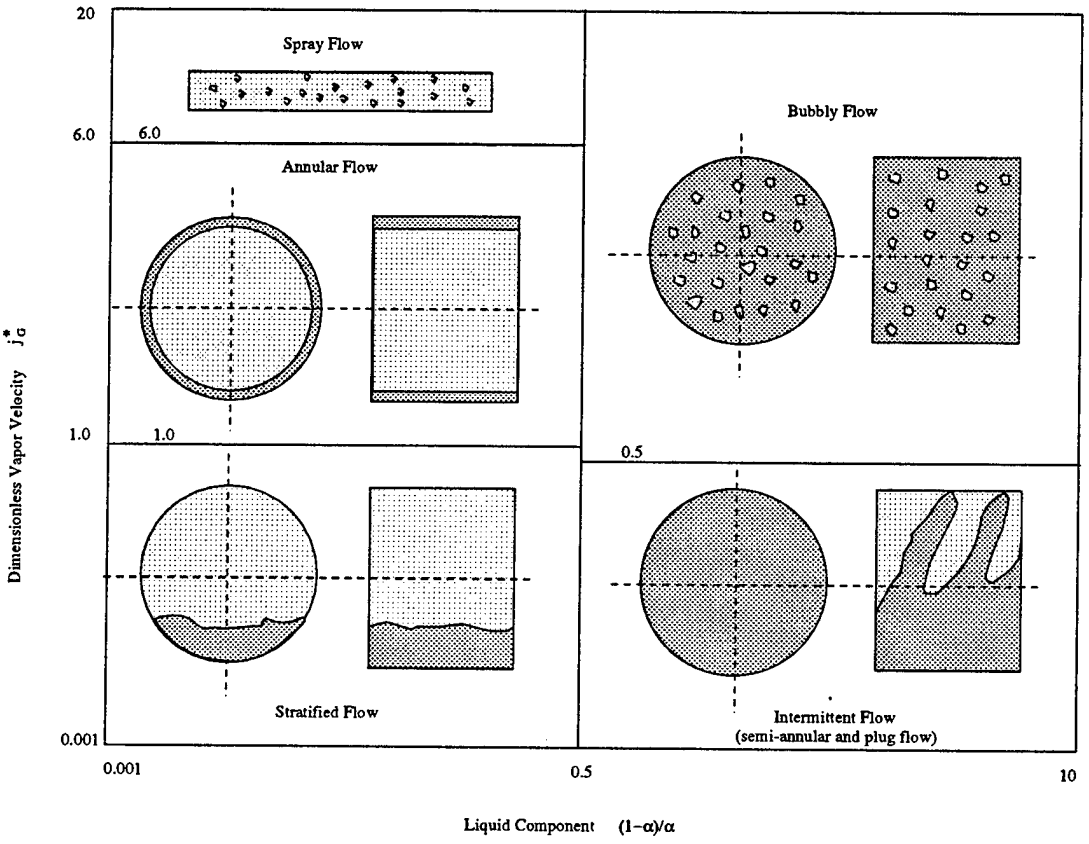

Figure 2.1. Flow Patterns of Condensation Inside Horizontal Tubes

The following reference values can be used to differentiate the types of flow [25]:

Stratified Flow: $j_G^* \leq 1, (1-\alpha)/\alpha \leq 0.5$

Annular Flow: $1 \leq j_G^* \leq 6, (1-\alpha)/\alpha \leq 0.5$

Spray Flow: $j_G^* \geq 6, (1-\alpha)/\alpha \leq 0.5$

Slug Flow: $j_G^* \leq 0.01, (1-\alpha)/\alpha \geq 0.5$

Semi-Annular Flow: $0.01 \leq j_G^* \leq 0.5, (1-\alpha)/\alpha \geq 0.5$

Bubble Flow: $j_G^* \geq 0.5, (1-\alpha)/\alpha \geq 0.5$

The most frequently occurring types of flow are stratified flow and annular flow. A large number of studies available in the literature concern these two kinds of condensation and their results will be presented in the following sections. It should be mentioned that spray flow condensation would definitely have a higher heat transfer coefficient than both stratified flow and annular flow condensation though no data for spray flow have been found in the literature.

2.3 Stratified Flow Condensation

Nusselt first proposed (in 1916) a simple theory for analyzing the laminar film condensation on a vertical flat surface [26]. The major assumptions made by Nusselt are that the film flow is laminar, the vapor is stagnant and exerts no drag on the downward motion of the condensate, and the heat transfer through the film is by conduction only. By solving the momentum equation separately and relating the solutions to a heat balance, Nusselt obtained the average Nusselt number as

$$\overline{Nu} = 0.943 \left(\frac{L}{k_f}\right) \left[\frac{g\rho_f(\rho_f - \rho_g)k_f^3 h_{fg}}{\mu_f L \Delta T}\right]^{1/4}. \tag{2.3}$$

Nusselt's film condensation theory has been found to under-predict the actual Nu in some situations. The discrepancy has been primarily attributed to the presence of waves on the film surface at low film Reynolds numbers, and the vapor shear stress at the vapor-condensate film interface at high film Reynolds numbers [27].

Condensation occurring inside a tube differs from that on a vertical flat surface in that the vapor entering the tube with some magnitude of velocity can exert a shear stress on the condensate film. For low vapor velocity, Chato's recommendation [28] for the average condensation Nusselt number inside a horizontal tube is

$$\overline{Nu} = 0.555 \left(\frac{D}{k_f}\right) \left[\frac{g\rho_f(\rho_f - \rho_g)k_f^3 h'_{fg}}{\mu_f D \Delta T}\right]^{1/4}, \tag{2.4}$$

where

$$h'_{fg} = h_{fg} + (3/8)c_{pf}\Delta T$$

is the revised enthalpy of vaporization. Chato's equation is limited to the Reynolds numbers of the inlet saturated vapor in the range $Re_{g,i} \leq 35,000$, where $Re_{g,i}$ is defined as

$$Re_{g,i} = \frac{u_{g,i} D}{\mu_{g,i}}. \tag{2.5}$$

Similarity can been seen between Chato's equation, Eq. (2.4), and Nusselt's equation, Eq. (2.3). An ideal stratified flow looks like that shown in Figure 2.2. Due to the low vapor velocity, gravity makes the condensate formed on the top of the inside surface of the tube flow off around the circumference downward the bottom. This process resembles that taking place on a vertical flat surface analyzed by Nusselt, except for the curvature of the inside surface of the tube. The different coefficients appearing in both equations, Eq. (2.3) and Eq. (2.4), represent this difference.

It should be noticed that stratified flow condensation does not depend on Reynolds number of the inlet saturated vapor or vapor velocity as seen in Eq. (2.4).

By far, Chato's equation, Eq. (2.4), is the most widely used correlation for stratified flow condensation.

2.4 Annular Flow Condensation

Another common type of film flow condensation, annular condensation, has been studied by a number of researchers. The transition from stratified flow to

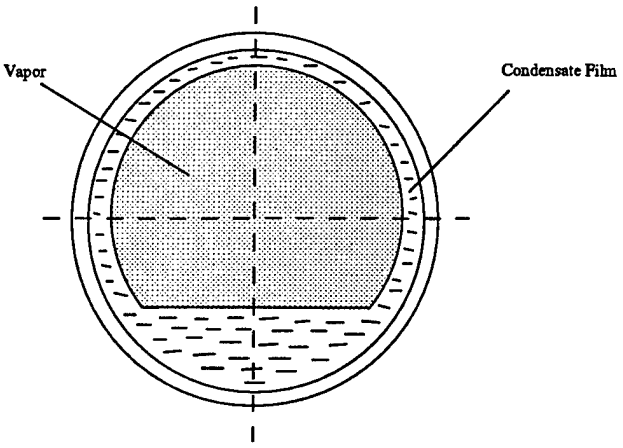

Figure 2.2. Stratified Film Condensation

annular flow is caused by the large vapor shear stress. There are five widely-used empirical or semiempirical correlations available in the literature for annular flow condensation.

Akers et al. [29, 30] used four dimensionless parameters to correlate the average Nusselt number as:

$$\overline{Nu} = f\left(Pr_f, Re_{g,eq}, \Delta T^*, Re_f\right), \tag{2.6}$$

where Pr_f is the condensate Prandtl number,

$$Re_{g,eq} = \frac{u_g D}{\mu_f}\left(\frac{\rho_f}{\rho_g}\right)^{1/2} \tag{2.7}$$

is the equivalent vapor Reynolds number,

$$\Delta T^* = \frac{h_{fg}}{c_{pf}\Delta T} \tag{2.8}$$

is the dimensionless subcooled temperature, and

$$Re_f = \frac{u_f D}{\mu_f} \tag{2.9}$$

is the film Reynolds number. If the film flow is laminar ($Re_f \leq 5{,}000$), Re_f is absent in Eq. (2.6); otherwise all four parameters should be employed.

Akers et al. [29, 30] obtained the following experimental correlation:

For laminar flow of the condensation film, that is $Re_f \leq 5,000$, when $1,000 \leq Re_{g,eq} \leq 20,000$, the average Nusselt number is

$$\overline{Nu} = 13.8 Pr_f^{1/2} \Delta T^{*1/6} Re_{g,eq}^{0.2}, \tag{2.10}$$

and when $20,000 \leq Re_{g,eq} \leq 100,000$,

$$\overline{Nu} = 0.1 Pr_f^{1/3} \Delta T^{*1/6} Re_{g,eq}^{2/3}. \tag{2.11}$$

For turbulent flow of the condensation film, that is $Re_f \geq 5,000$,

$$\overline{Nu} = 0.026 Pr_f^{1/3} (Re_{g,eq} + Re_f)^{0.8}, \tag{2.12}$$

when $Re_{g,eq} \geq 20,000$.

The second correlation for the local Nusselt number of annular film condensation is that of Soliman et al. [31]:

$$Nu = 0.036 \frac{Pr_f^{0.65} D \rho_f^{1/2}}{\mu_f} F_o^{1/2}, \tag{2.13}$$

where F_o is the wall shear stress that is defined as $F_o = F_f + F_m$, where:

$$\begin{aligned} \frac{F_f}{8\dot{m}^2/\pi^2 \rho_g D^4} &= 0.045 Re_{g,t}^{-0.2} \left[x^{1.80} + 5.70 \left(\frac{\mu_f}{\mu_g} \right)^{0.523} (1-x)^{0.470} x^{1.33} \left(\frac{\rho_g}{\rho_f} \right)^{0.261} \right] \\ &\quad + 0.045 Re_{g,t}^{-0.2} \left[8.11 \left(\frac{\mu_f}{\mu_g} \right)^{0.105} (1-x)^{0.940} x^{0.860} \left(\frac{\rho_g}{\rho_f} \right)^{0.522} \right], \end{aligned}$$

and

$$\frac{F_m}{8\dot{m}^2/\pi^2 \rho_g D^4} = -0.50 \left(\frac{D}{L} \right) \left[(2x - 1 - \beta x) \left(\frac{\rho_g}{\rho_f} \right)^{1/3} + \left(\frac{1}{x} - 3 + 2x \right) \left(\frac{\rho_g}{\rho_f} \right)^{4/3} \right]$$

$$-0.50 \left(\frac{D}{L} \right) \left[2(1-x) \left(\frac{\rho_g}{\rho_f} \right)^{2/3} + \left(2\beta - \frac{\beta}{x} - \beta x \right) \left(\frac{\rho_g}{\rho_f} \right)^{5/3} + 2(1 - x - \beta + \beta x) \frac{\rho_g}{\rho_f} \right],$$

where β is a constant relating interfacial liquid velocity to the average velocity throughout the condensate film, and

$$Re_{g,t} = \frac{u_m D}{\mu_g} \tag{2.14}$$

is the Reynolds number based on total flow rate and local vapor density.

The third correlation for the average Nusselt number of annular film condensation of steam was proposed by Boyko and Kruzhilin [32]:

$$\overline{Nu} = 0.024 Re_{f,t}^{0.8} Pr_f^{0.43} \frac{(\rho/\rho_m)_i^{1/2} + (\rho/\rho_m)_o^{1/2}}{2}, \tag{2.15}$$

where

$$\frac{\rho}{\rho_m} = 1 + \left(\frac{\rho_f - \rho_g}{\rho_g}\right) x,$$

and

$$Re_{f,t} = \frac{u_m D}{\mu_f} \tag{2.16}$$

is the Reynolds number assuming all mass would flow as liquid.

Traviss et al. [33] reported the following correlation for the local Nusselt number:

$$Nu = \frac{1}{F_2} 0.15 \left(\frac{\rho_f}{\rho_g}\right)^{1/2} c_{pf} \mu_g^{0.1} \frac{G^{0.9}}{D^{1.1}} x^{0.9} k_f \left[1 + 2.85 \left[\left(\frac{\mu_f}{\mu_g}\right)^{0.1} \left(\frac{1-x}{x}\right)^{0.9} \left(\frac{\rho_g}{\rho_f}\right)^{0.5}\right]^{0.523}\right] \tag{2.17}$$

where

$$F_2 = 0.707 Pr_f Re_{f,eq}^{0.5}$$

for $Re_{f,eq} < 50$,

$$F_2 = 5Pr_f + 5ln[1 + Pr_f(0.09636 Re_{f,eq}^{0.585} - 1)]$$

for $50 < Re_{f,eq} < 1125$,

$$F_2 = 5Pr_f + 5ln(1 + 5Pr_f) + 2.5ln(0.00313Re_{f,eq}^{0.812})$$

for $Re_{f,eq} > 1125$, and $Re_{f,eq}$ is the equivalent Reynolds number defined as

$$Re_{f,eq} = \frac{u_m D}{\mu_f}(1 - x). \tag{2.18}$$

In addition to the above four correlations, Shah [34] proposed a simple equation which is considered to cover the widest range of experimental data. This equation represents measurements with water, $R-11$, $R-12$, $R-113$, methanol, ethanol, benzene, toluene, and trichloroethylene during condensation in vertical, horizontal, and inclined tubes with inside diameters of 7.4 to 40mm. The range of experimental parameters includes the reduced pressure $0.002 \leq p_r \leq 0.44$, saturated temperature $21°C \leq T_{sat} \leq 310°C$, vapor velocity $3m/s \leq u_g \leq 300m/s$, mass flowrate $10.8kg/s-m^2 \leq G \leq 210.6kg/s-m^2$, heat flux $158W/m^2 \leq \dot{q} \leq 1.893 \times 10^6 W/m^2$, Reynolds number $100 \leq Re_{f,t} \leq 63,000$, Prandtl number $1 \leq Pr \leq 13$, and vapor quality $0\% \leq x \leq 100\%$. The mean error of this equation is $\pm 15.4\%$. The following is the Shah's equation for the average Nusselt number:

$$\overline{Nu} = \frac{0.023 Re_{f,t}^{0.8} Pr_f^{0.4}}{x_2 - x_1}\left[-\frac{(1-x)^{1.8}}{1.8} + \frac{3.8}{p_r^{0.38}}\left(\frac{x^{1.76}}{1.76} - \frac{0.04x^{2.76}}{2.76}\right)\right]_{x_1}^{x_2}, \tag{2.19}$$

where p_r is the reduced pressure of vapor, and $Re_{f,t}$ is the Reynolds number defined in Eq. (2.16).

2.5 Two Phase Pressure Drop

Two-phase pressure drop in a horizontal tube is the result of the action of two factors: the friction force and momentum changes. The general equation is

$$\Delta P = \Delta P_f + \Delta P_m. \tag{2.20}$$

The pressure drop due to momentum changes is given by

$$\Delta P_m = \frac{\dot{m}^2}{A_0^2}(v_o - v_i). \tag{2.21}$$

At pressures close to one atmosphere for a very wide variety of liquids, the Lockhart and Martinelli method [35, 36] is considered to be the best in calculating two phase friction pressure drop. The friction pressure drop is determined by first calculating the pressure drop for either the liquid flowing alone, or the gas flowing alone in the tube at the single species mass flowrate. That is

$$\Delta P_{f,g} = f\left(\frac{L}{D}\right)\frac{\dot{m}_g{}^2 v_g}{2A_0^2}, \tag{2.22}$$

or

$$\Delta P_{f,f} = f\left(\frac{L}{D}\right)\frac{\dot{m}_f{}^2 v_f}{2A_0^2}. \tag{2.23}$$

In the above two equations, f is the friction factor that is determined from the Moody chart. The two-phase friction pressure drop is then obtained by multiplying either the liquid-only pressure drop, or the gas-only pressure drop, by the appropriate multiplier ϕ_g or ϕ_f. That is

$$\Delta P_f = \phi_g^2 \Delta P_{f,g}, \tag{2.24}$$

or

$$\Delta P_f = \phi_f^2 \Delta P_{f,f}. \tag{2.25}$$

The multiplier (ϕ_g or ϕ_f) is a function of X that depends on the flow mechanism of both the liquid flowing alone and the gas flowing alone. ϕ_g or ϕ_f can be obtained either from the Lockhart and Martinelli chart or from the Lockhart and Martinelli data [35, 36] once X is determined from

$$X^2 = \frac{Re_g^m}{Re_f^n}\frac{C_f}{C_g}\left(\frac{\dot{m}_f}{\dot{m}_g}\right)^2 \frac{v_f}{v_g}, \tag{2.26}$$

where coefficients m, n, C_f, and C_g are determined from Table 2.1.

Table 2.1. Lockhart and Martinelli Constants

Constant	Laminar Regime $Re_g(or Re_f) \leq 2,500$	Turbulent Regime $2,500 \leq Re_g(or Re_f) \leq 50,000$
C_f	64	0.316
C_g	64	0.316
m	1	0.25
n	1	0.25

2.6 Summary

The above sections have offered a total of six Nu correlations available in the literature for calculating film condensation heat transfer inside macrotubes, one for stratified flow, and five for annular flow. They are seen to be very cumbersome to use, and moreover they are generally coupled with pressure drops. Therefore, some useful points are summarized here for the research of macrotube condensation as follows:

1. The minimum inside diameter of macrotubes used to acquire those six heat transfer correlations is $7.4mm$.

2. There are up to six types of Reynolds numbers defined and used (Eq. (2.5), Eq. (2.7), Eq. (2.9), Eq. (2.14), Eq. (2.16), and Eq. (2.18)) to relate Nusselt numbers. Since these different types of Reynolds number are usually not compatible with each other, the different results of Nusselt numbers reported are difficult to compare.

3. Eight dimensionless parameters are used to relate Nusselt numbers. These Nusselt numbers may be expressed symbolically as

$$Nu \text{ or } \overline{Nu} = f(six\ types\ of\ Re, x, \Delta T^*, p_r, d/L, Pr, \rho_g/\rho_f, \mu_g/\mu_f). \quad (2.27)$$

4. The correlation for stratified flow condensation (Eq. (2.4)) is independent of Reynolds numbers or velocities of the inlet saturated vapor. The five

correlations for annular flow condensation (Eq. (2.10-2.12), Eq. (2.13), Eq. (2.15), Eq. (2.17), and Eq. (2.19)) all depend on Reynolds number.

5. Spray flow condensation should have a higher heat transfer coefficient than both stratified and annular condensation though no correlations for this type of condensation are available in the literature.

6. The vapor quality is present in all the five correlations for annular flow condensation (Eq. (2.10-2.12), Eq. (2.13), Eq. (2.15), Eq. (2.17), and Eq. (2.19)).

7. The heat transfer and pressure drops are generally coupled.

8. Due to the change of vapor quality along the length of a tube, a numerical integration must generally be executed between the inlet and outlet of the tube to acquire the overall two-phase pressure drop and the average Nusselt number from the correlations for the local Nusselt number. That is, the tube is discretized into a series of short sections and the separate contributions of pressure drop and heat transfer of each section are summed.

9. Errors for all those heat transfer correlations are reported to be quite large. A 100% or even larger error is a common situation [36, 37].

10. The effect of Reynolds number on Nusselt number is observable only for a large Re range. For instance, the Re range in Akers et al. [29, 30] is $10^3 \leq Re \leq 10^5$. This result is due to the large uncertainty associated with condensation experiments which tends to mask the Re effect when only a small Re range is considered. For microscale tube condensation, the Re range is expected to be small (i.e., $500 \leq Re \leq 5,000$) due to pressure drop constraints that may make it difficult to observe the Re effect on Nu.

CHAPTER 3

EXPERIMENTS AND MODELING

The objective of the current research is to experimentally investigate the heat transfer and pressure drop of steam condensation inside a horizontal microtube. This chapter will describe the experimental apparatus and procedure. Then, correlations of the data for average Nusselt number and pressure drop will be derived.

3.1 Experimental Apparatus

The experimental apparatus is shown schematically in Figure 3.1, and a photograph of this experimental apparatus is shown in Figure 3.2. There are two loops in the apparatus. The first flow loop is used to supply water (from the building supply) that is to be condensed after it is heated to superheated steam. The second loop is used to supply the cooling water, also from tap water, that is used to cool the microtube in which condensation is taking place. All tubes in the two loops are stainless steel with 6.35mm (0.25in) outside diameter. The two streams of the tap water are filtered by two $7\mu m$ filters, respectively, before the water enters each loop. The microtube has inside diameter of $250\mu m$, outside diameter of $790\mu m$, and length of $48mm$. Table 3.1 lists the main performance data of instruments used in the experiment.

The superheat temperature of steam at the inlet of the microtube is controlled by a combination of a temperature controller and pressure transducer. The temperature controller is connected to a thermocouple that measures the temperature of steam at the inlet of the microtube. This temperature is fed back to control the on-off of a rope heater. The pressure transducer measures gauge pressure and thus the absolute pressure at the the inlet of the microtube is obtained by adding the inlet gauge pressure to the outlet absolute pressure that is equal to the

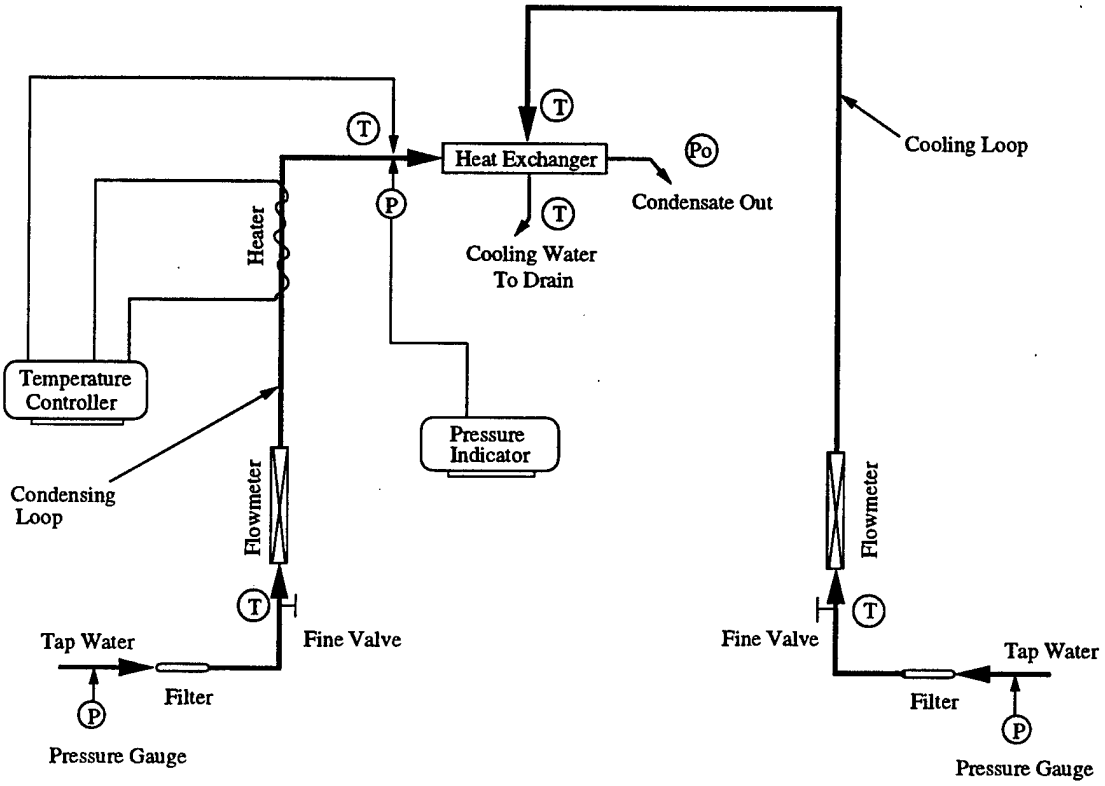

Figure 3.1. Schematic of Experimental Apparatus

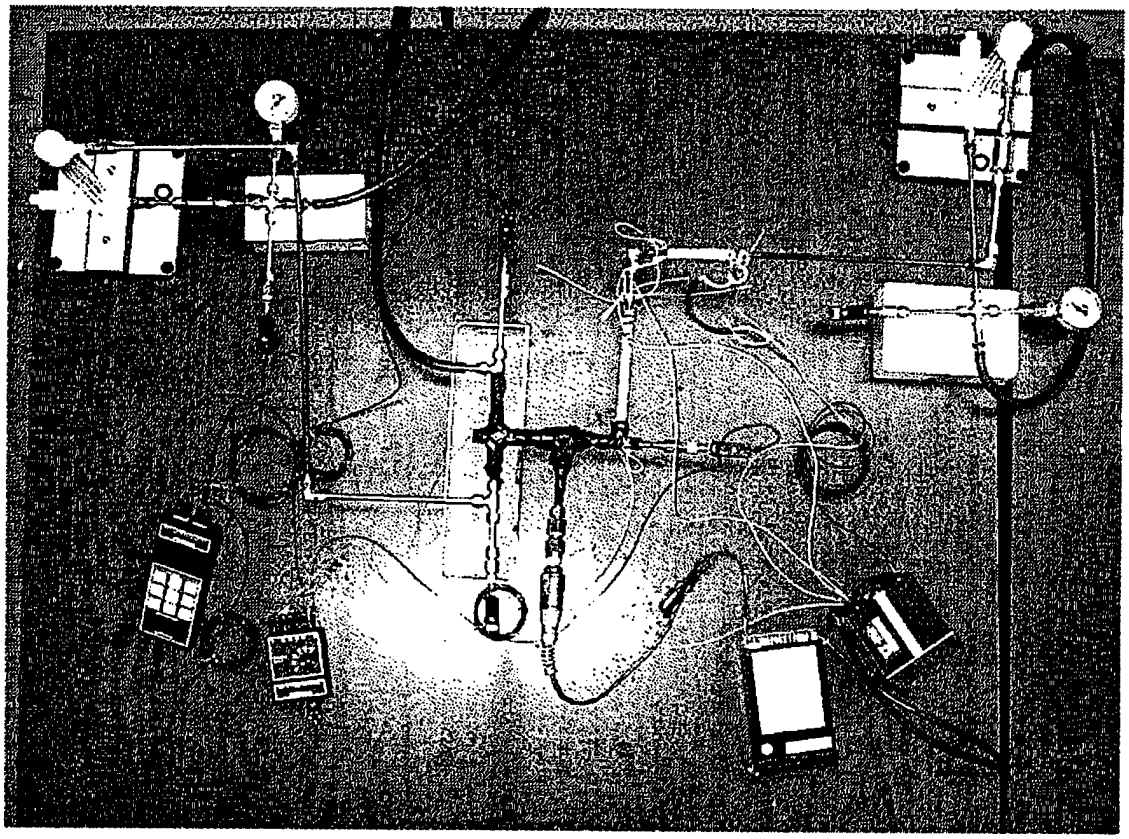

Figure 3.2. Photograph of Experimental Apparatus

Table 3.1. Limiting Conditions of Main Equipment

Component Name, Type and Maker	Pressure PSI (kPa)	Temperature ($°C$)	Flow Rate (ml/min)	Accuracy
Pressure Transducer PX202-015GV OMEGA	15(103)	$-40 \sim 125°C$	N/A	±0.25%
Pressure Indicator DP41-S OMEGA	N/A	N/A	N/A	$1\mu V$
Thermocouple 5TC-TT-J-36-36 OMEGA	N/A	(Type J)	N/A	$\pm 0.1\% reading$ $+0.6°C$
Thermal Meter HH23 OMEGA	N/A	N/A	N/A	$\pm 0.1\% reading$ $+0.6°C$ (including thermocouple)
Temperature Controller CN3240 OMEGA	N/A	$-73 \sim 760°C$	N/A	$\pm 0.14\% of span$ + 1 digital
Flow Meter (Condensing Loop) GF7060 GILMONT	125 (862)	N/A	$0.0091 \sim 1.28(Glass)$ $0.0576 \sim 5.49(S.S.)$	$\pm 2\% reading$
Flow Meter (Cooling Loop) GF7160 GILMONT	125 (862)	N/A	$0.0212 \sim 4.50(Glass)$ $0.115 \sim 16.6(S.S.)$	$\pm 2\% reading$
Pressure gauge PGC-20L-100 OMEGA	100(690)	N/A	N/A	N/A

atmospheric pressure in the test field (the outlet of the microtube is open to the atmosphere). The atmosphere pressure is determined by using a barometer placed in the test field. Volumetric flowrates of tap water for both loops are measured by two fine float flowmeters, respectively. Figure 3.3, Figure 3.4 and Figure 3.5 depict the heat exchanger in which condensation occurs. The heat exchanger is a non-mixing cross-flow heat exchanger. The outside shell is a Swagelok cross fitting, and the inside tube is the microtube being studied. The cooling water flows over the microtube. The amount of condensed heat removed is calculated using the change of enthalpy of the cooling water. Two thermocouples located at the inlet and outlet of the heat exchanger, respectively, measure temperatures that are used to calculate the change of enthalpy of the cooling water. The outside surface of the heat exchanger is well-insulated by the wrapped insulation tape, thus heat loss through the heat exchanger may be ignored.

Outside wall temperatures of the microtube are measured by four fine ther-

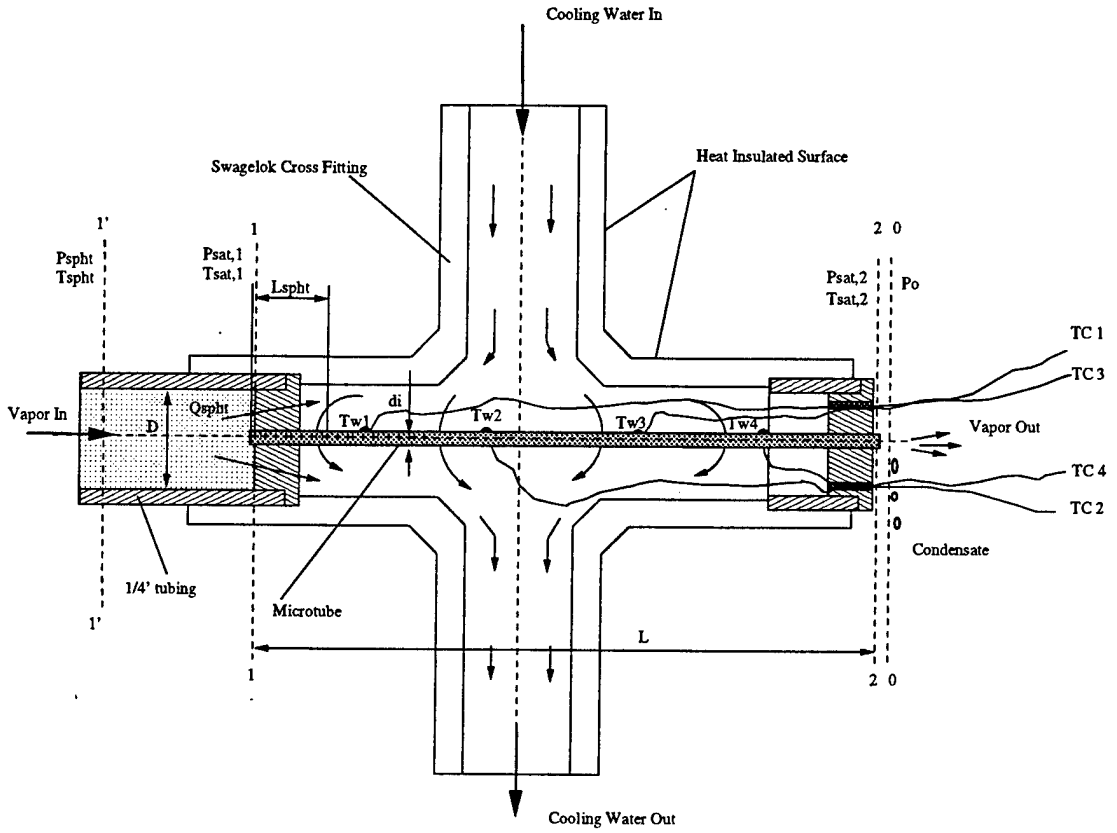

Figure 3.3. Schematic of Heat Exchanger

mocouples that are glued to the microtube outside wall and are equally spaced along the flow direction. The significant error of measurement of the outside wall temperatures may be ignored because the bead diameter of those fine thermocouples ($127\mu m$) is small enough compared to the outside diameter of the microtube ($790\mu m$). All thermocouples used in the experiment are connected to a thermal meter.

3.2 Experimental Procedure

The experiments are conducted according to the following procedure:

1. Evacuate air in the condensing loop by letting the tap water flow through the loop at a large flow rate for a long period of time (approximately 5 minutes).

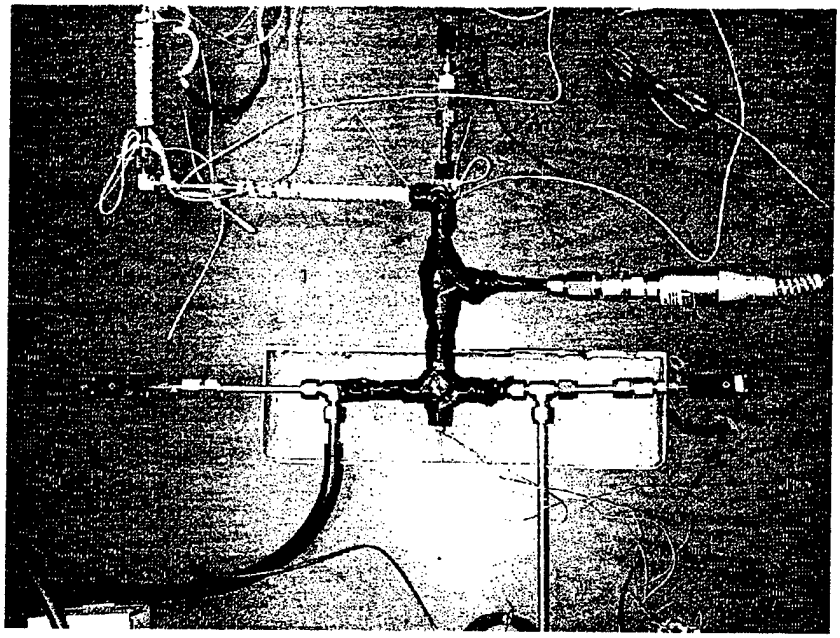

Figure 3.4. Photograph of a Portion of Experimental Apparatus

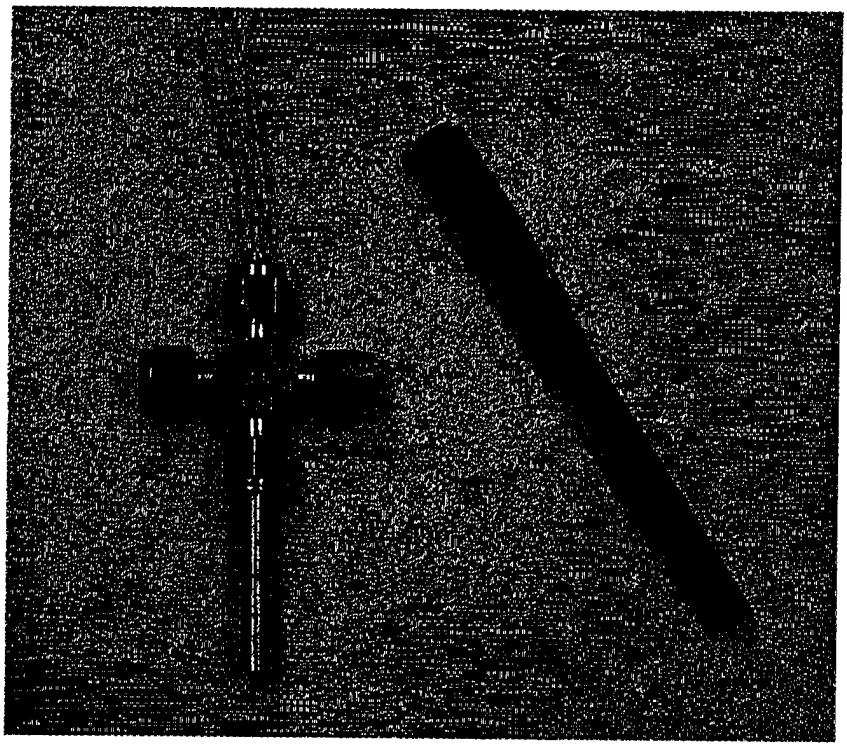

Figure 3.5. Photograph of Heat Exchanger

2. Set the volumetric flowrate into the condensing loop at a fixed value such that an expected Reynolds number ($Re_{g,i}$) of inlet saturated vapor is achieved. The expected range of $Re_{g,i}$ is approximately from 500 to 5,000.

3. Regulate the volumetric flowrate into the cooling loop such that an expected vapor quality (x_2) at the outlet of the microtube is achieved at the fixed $Re_{g,i}$. The expected range of x_2 is approximately from 0.1 to 0.9.

4. Obtain an expected superheat temperature of the inlet vapor by setting a value of the temperature controller, in comparison with the reading of the pressure transducer. The superheat temperature of the inlet vapor is controlled to be less than $25°C$.

5. Collect data when a steady state has been achieved. Collected data include those which will be shown in next section.

6. Change the volumetric flowrate into the condensing loop to another value which corresponds to another $Re_{g,i}$.

7. Repeat steps 2 $\sim$ 6 until all the values of the expected $Re_{g,i}$ and x_2 are considered.

3.3 Experimental Modeling

3.3.1 Directly Measurable Quantities in the Experiment

Referring to Figure 3.1 and Figure 3.3, 15 parameters are directly measurable by means of the data acquisition instruments. These 15 parameters are shown in Table 3.2.

3.3.2 Inlet Vapor Quality and Thermodynamic Process of Steam

The steam is heated to a superheated state to ensure that only vapor is introduced to the microtube where condensation occurs. Referring to Figure 3.3, an assumption is made that the wall between the supply tubing and the microtube is ideally thermally insulated, then the superheated steam will, when condensed

Table 3.2. Directly Measurable Quantities in the Experiment

No.	Variable	Description
1	d_i	inside diameter of the microtube
2	d_o	outside diameter of the microtube
3	L	length of the microtube
4	D	inside diameter of the supply tubing
5	$T_{w,i}$	inlet temperature of water into both loops
6	$T_{w,o}$	cooling water temperature at the outlet of the heat exchanger
7	T_{spht}	superheat temperature of steam
8	$T_{wl,o,1}$	wall temperature of the microtube at point 1 (Figure 3.2)
9	$T_{wl,o,2}$	wall temperature of the microtube at point 2 (Figure 3.2)
10	$T_{wl,o,3}$	wall temperature of the microtube at point 3 (Figure 3.2)
11	$T_{wl,o,4}$	wall temperature of the microtube at point 4 (Figure 3.2)
12	P_o	atmospheric pressure
13	P_{spht}	gauge pressure of steam in the inlet of the microtube
14	$\dot{V}_{cd}$	volumetric flowrate of water entering the condensation loop
15	$\dot{V}_w$	volumetric flowrate of water entering the cooling loop

inside the microtube, arrive at a saturated vapor state somewhere downstream close to the inlet of the microtube. Let us call this length the superheated length, L_{spht}, which is marked in Figure 3.3. Due to the good thermal conductivity of the stainless steel wall between the supply tubing and the microtube, there would be some unavoidable amount of heat entering the cooling water through the wall. Accordingly, the superheated length, L_{spht}, would be reduced in the actual situation. If the superheat temperature of the inlet vapor is not too high, L_{spht} would be very close to zero and the location where the saturated vapor state of steam is achieved would be very close to the inlet of the microtube. In the experiment, the superheat temperature will be controlled to be less than $25°C$. Under this limiting value, the following calculation will show that L_{spht} is so small that it can be assumed to be zero.

It is assumed that:

1. the wall between the supply tubing and the microtube is ideally thermally insulated,

2. the condensation heat removal along the length of the microtube is uniform,

3. the absolute pressure across the microtube is 0.1MPa,

4. the superheat temperature of steam at the inlet of the microtube (point 1′) is 25^oC,

5. the vapor quality (x_2) at the outlet of the microtube (point 2) is from 0.2 to 0.8, and

6. the change of kinetic energy from point 1′ to point 1 is ignored.

With these conditions, we have

$$\begin{aligned}
\frac{L_{spht}}{L} &\approx \frac{\dot{Q}_{spht}}{\dot{Q}_t} \\
&= \frac{\dot{m}_{cd}(h_1 - h_{sat,1})}{\dot{m}_{cd}(h_1 - h_2)} \\
&= \frac{h_1 - h_{sat,1}}{h_1 - h_2} \\
&= \frac{h_1 - h_{sat,1}}{(h_1 - h_{sat,1}) + (h_{sat,1} - h_2)} \\
&= \frac{h_1 - h_{sat,1}}{(h_1 - h_{sat,1}) + [h_{sat,1} - (h_{sat,f2} + x_2 h_{sat,fg2})]} \\
&\approx \frac{50}{50 + [2675 - (417 + 0.8 \times 2258)]} \\
&= 10.0\%, \qquad (3.1)
\end{aligned}$$

where values of enthalpy of steam are taken from [38], and x_2 is assumed to be 0.8 which would be the worst situation.

It is noticed that the above calculation is based on the ideal insulation assumption (see assumption 1). However, the actual process with nonideal insulation would reduce the superheated length to a smaller value. Therefore, it seems to be a reasonable assumption that the steam achieves a saturated state at the inlet (point 1) of the microtube, that is, the inlet vapor quality $x_1 \approx 100\%$.

On the other hand, for the sake of accuracy, the amount of heat required for condensation between the inlet (point 1) and outlet (point 2) of the microtube,

which will be used to calculate average condensation Nusselt numbers, should be obtained by deducting the heat gain through the wall between the supply tubing and the microtube from the total amount of heat removed by the cooling water.

The process from point 1′ to point 1 is a single phase process in which the superheated vapor state at point 1′ changes to saturated vapor state at point 1.

The process from point 2 to point 0 is a process of two phase flow without phase change, in which the steam jets into the atmosphere from the outlet of the microtube. It is assumed that the distance between point 2 and point 0 is so short that this process can be considered to be thermally insulated from the atmosphere. It is also reasonable to assume that the cross-sectional area of stream of the steam at point 0 is the same as that of the microtube (A_0), and the absolute pressure at point 0 is equal to the atmospheric pressure.

It is noticed that there will be a sudden contraction for the fluid from point 1′ to point 1 and a sudden expansion from point 2 to point 0. Therefore, the overall thermodynamic process that the steam undergoes from point 1′ to point 0 should be:

1. from point 1′ to point 1: single phase heat transfer without phase change, a sudden contraction of flow involved.

2. from point 1 to point 2: condensation phase change.

3. from point 2 to point 0: two phase adiabatic flow without phase change, a sudden expansion of flow involved.

The following is the derivation of data reduction equations for $\overline{Nu}$, x_2, and ΔP. It will be seen from these equations that they are coupled.

3.3.3 Pressure Drop

Applying an energy balance between point 1′ and point 1 (see Figure 3.3) gives an equation for the saturated vapor pressure ($P_{sat,1}$) at the inlet of the microtube:

$$P_{spht} + \frac{u_1^2}{2v_1} = P_{sat,1} + (1 + K_c)\frac{u_{sat,1}^2}{2v_{sat,1}}, \tag{3.2}$$

where K_c is the contraction coefficient due to the sudden contraction from diameter D to d_i. Empirical correlations are available for K_c, such as one presented by White [39]:

$$K_c = 0.42\left(1 - \frac{d_i^2}{D^2}\right). \tag{3.3}$$

Based on mass continuity of steam,

$$\frac{u_{sat,1}}{u_1} = \frac{A_1 v_{sat,1}}{A_0 v_1}, \tag{3.4}$$

and the velocity of superheated steam, u_1, is given by

$$u_1 = \frac{\dot{m}_{cd} v_1}{A_1}. \tag{3.5}$$

The saturated vapor pressure at the inside inlet of the microtube is obtained by inserting Eqs. (3.3), (3.4), and (3.5) into Eq. (3.2):

$$P_{sat,1} = P_{spht} - \frac{1}{2v_1}\left(\frac{\dot{m}_{cd} v_1}{A_1}\right)^2 \left[(1 + K_c)\left(\frac{v_{sat,1}}{v_1}\right)\left(\frac{A_1}{A_0}\right)^2 - 1\right]. \tag{3.6}$$

In order to find the pressure ($P_{sat,2}$) at the outlet of the microtube, the vapor quality at the outlet of the microtube must be determined first. By applying an energy balance between point 1′ and point 0 (see Figure 3.2), we have

$$\dot{m}_{cd}(h_1 + \frac{u_1^2}{2}) = \dot{Q}_t + \dot{m}_{cd}(h_{sat,0} + \frac{u_0^2}{2}), \tag{3.7}$$

where $\dot{Q}_t$ is the total rate of heat removed by the cooling water, that is

$$\dot{Q}_t = \dot{m}_w(h_{w,o} - h_{w,i}). \tag{3.8}$$

Mass continuity of the steam yields

$$\frac{u_0}{u_1} = \frac{A_1 v_{sat,0}}{A_0 v_1}, \tag{3.9}$$

where $v_{sat,0}$ is the specific volume at point 0 that is given by

$$v_{sat,0} = v_{sat,f0} + x_0 v_{sat,fg0}, \tag{3.10}$$

and the velocity, u_1 in Eq. (3.7), has been determined by Eq. (3.5). The enthalpy at point 0 is

$$h_{sat,0} = h_{sat,f0} + x_0 h_{sat,fg0}. \tag{3.11}$$

By substituting Eqs. (3.8) to Eq. (3.11) into Eq. (3.7), x_0 can be determined from the following equation:

$$a_1 x_0^2 + a_2 x_0 + a_3 = 0, \tag{3.12}$$

where a_1, a_2, and a_3 are three constants:

$$a_1 = \frac{1}{2}\left(\frac{\dot{m}_{cd} v_{sat,fg0}}{A_0}\right)^2,$$

$$a_2 = h_{sat,fg0} + \left(\frac{\dot{m}_{cd}}{A_0}\right)^2 (v_1 v_{sat,f0} v_{sat,fg0}),$$

$$a_3 = \left(\frac{\dot{m}_{cd}}{\dot{m}_w}\right)(h_{w,o} - h_{w,i}) + h_{sat,f0} - h_1 - \frac{1}{2}\left(\frac{\dot{m}_{cd} v_1}{A_1}\right)^2 + \frac{1}{2}\left(\frac{\dot{m}_{cd} v_{sat,f0}}{A_0}\right)^2.$$

The equation for the pressure ($P_{sat,2}$) at the outlet of the microtube is obtained by applying the energy balance between point 2 and point 0:

$$P_{sat,2} + \frac{u_{sat,2}^2}{2v_{sat,2}} = P_0 + \frac{u_0^2}{2v_{sat,0}} + K_e \frac{u_{sat,2}^2}{2v_{sat,2}}, \tag{3.13}$$

where K_e is the expansion coefficient due to the sudden expansion from diameter d_i to the infinite space (the atmosphere), which is determined to be [39]

$$K_e = 1. \tag{3.14}$$

The velocity, u_0 in Eq. (3.13), is given by

$$u_o = \frac{\dot{m}_{cd} v_{sat,0}}{A_0}. \tag{3.15}$$

By considering Eq. (3.10), and combining Eqs. (3.14) and (3.15) into Eq. (3.13), we obtain

$$P_{sat,2} = P_0 + \frac{1}{2(v_{sat,f0} + x_0 v_{sat,fg0})} \left[\left(\frac{\dot{m}_{cd}}{A_0} \right) (v_{sat,f0} + x_0 v_{sat,fg0}) \right]^2. \tag{3.16}$$

The condensation pressure drop is then acquired from Eq. (3.6) and Eq. (3.16):

$$\Delta P_{cd} = P_{sat,1} - P_{sat,2}. \tag{3.17}$$

3.3.4 Outlet Vapor Quality

The result for vapor quality (x_2) at the inside outlet of the microtube is obtained directly from an energy balance between point 2 and point 0, that is

$$x_2 = \frac{h_{sat,f0} + x_0 h_{sat,fg0} - h_{sat,f2}}{h_{sat,fg2}}. \tag{3.18}$$

It is noticed that both $h_{sat,f2}$ and $h_{sat,fg2}$ are a function of $P_{sat,2}$, which has been determined in Eq. (3.16).

3.3.5 Nusselt Number

Finally, the condensation average Nusselt number is determined from the following definition:

$$\overline{Nu} \equiv \frac{\overline{h} d_i}{\overline{k}_f}, \tag{3.19}$$

where $\overline{h}$ is the average heat transfer coefficient determined from

$$\overline{h} = \frac{\dot{Q}_t - \dot{Q}_{spht}}{\pi d_i L \Delta T}, \tag{3.20}$$

where $\dot{Q}_{spht}$ is the rate of heat into the cooling water from the wall between the supply tubing and the microtube as explained previously. $\dot{Q}_{spht}$ can be determined from an energy balance between point 1′ and point 1:

$$\dot{Q}_{spht} = \dot{m}_{cd}\left[h_1 - h_{sat,1} + \frac{u_1^2}{2}\left[1 - \left(\frac{u_{sat,1}}{u_1}\right)^2\right]\right]. \tag{3.21}$$

In Eq. (3.20), ΔT is the average subcooled temperature given by

$$\Delta T = \frac{T_{sat,1} + T_{sat,2}}{2} - \overline{T}_{wl,i}, \tag{3.22}$$

where the inside wall mean temperature of the microtube $\overline{T}_{wl,i}$ can be obtained from the measured outside wall temperatures by considering the thermal conduction between the inside wall and outside wall of the microtube:

$$\overline{T}_{wl,i} = \frac{1}{4}\sum_{j=1}^{4}(T_{wl,o,j}) + (\dot{Q}_t - \dot{Q}_{spht})\frac{ln(d_o/d_i)}{2\pi\overline{k}_{wl}L}. \tag{3.23}$$

The average Nusselt number is determined by combining Eqs. (3.20), (3.21), (3.22) and (3.23) into Eq. (3.19).

CHAPTER 4

RESULTS AND DISCUSSION

The macroscale empirical and semiempirical correlations that are most widely used for film condensation in horizontal tubes have been presented in Chapter 2. This chapter will first compare these correlations with the results obtained in the current experiment. After a comparison is made, a significant deviation between them will be seen. On the other hand, it will be seen that conventional methods for Nusselt number correlations seem not to work for the current experimental results. It is found that the correlated Nusselt numbers in the current research are dependent on one parameter only instead of many parameters as is expected. Some attempts to explain these significant differences will be presented in the latter part of this chapter.

4.1 Ranges of Experimental Parameters

Forty six sets of data have been collected and are listed in Appendix B. Ranges of experimental parameters are shown in Table 4.1. The superheat temperature of steam (T_{spht}) at the inlet of the microtube is on the order of $25^{o}C$, indicating that it is reasonable to employ the assumption that the inlet vapor quality (x_1) is 100% as discussed in Chapter 3. The velocity of the inlet saturated vapor ($u_{g,i}$) is up to $276m/s$ that may cause heating effects. This will be discussed later in this chapter.

4.2 Flow Patterns Based on the Macroscale Method

One method to determine the flow pattern in the current experiment is from the flow pattern map shown in Figure 2.1. From the values of the dimensionless vapor velocity j_G^* and liquid component $(1-\alpha)/\alpha$ in Table 4.1, it is seen that current

Table 4.1. Ranges of Experimental Parameters

$Re_{g,i}$	$393 \sim 4683$	x_1	$100(\%)$
$u_{g,i}$	$33 \sim 276(m/s)$	x_2	$24.3 \sim 94.2(\%)$
ΔT	$6.3 \sim 21.3(°C)$	j_G^*	$14.8 \sim 150.9$
T_{spht}	$12.2 \sim 24.5(°C)$	$(1-\alpha)/\alpha$	$2.3 \times 10^{-4} \sim 41 \times 10^{-4}$
ΔP	$-3.4 \sim 65.3(kPa)$		

experimental results should be located in the regime of spray flow. On the other hand, Chato recommended [28] that for stratified flow, Reynolds numbers of inlet saturated vapor be $Re_{g,i} \leq 35,000$. From this, the current experimental results would most likely be in the stratified flow regime. Because the experimental or theoretical correlations of Nusselt numbers for spray flow are non-existent in the literature, and because the annular flow regime is located between the stratified flow and spray flow regimes as shown in Figure 2.1, it should be reasonable to choose available correlations from both stratified flow and annular flow as references for comparing current experimental results. Note that no attempt was made to verify visually the type of flow that occurred in the tests.

4.3 Comparisons of Experimental Results with Macroscale Correlations

The experimental results for Nusselt numbers, pressure drops, and outlet vapor quality are acquired based on the models established in the Chapter 3. Properties of water are obtained by a curve-fitting program that takes data from the property tables in the literature [38, 40]. The formulas used for the curve-fittings are polynomials. The order of each polynomial is determined based on (1) the range of data to be used, (2) the nature of the data in the tables, and (3) a trial-and-error basis. Properties of stainless steel of the microtube being studied are from MicroGroup, Inc. [41].

4.3.1 Nusselt Number

Four empirical and semiempirical correlations for film condensation Nusselt numbers have been chosen to make comparison with current experimental results. Refer to Chapter 2 where the correlations that are most widely used in the literature have been presented. The chosen correlations for this comparison include those of Chato [28], Akers et al. [29, 30], Boyko et al. [32], and Shah [34]. It is noticed that the correlation of Chato is suitable for film condensation in stratified flow in horizontal tubes, and the other three correlations chosen here are for annular flow in horizontal or nonhorizontal tubes. As mentioned above, it is unclear which types of film condensation occurred in the current experiment, therefore the above correlations which cover a wide range from stratified flow to annular flow are accordingly selected.

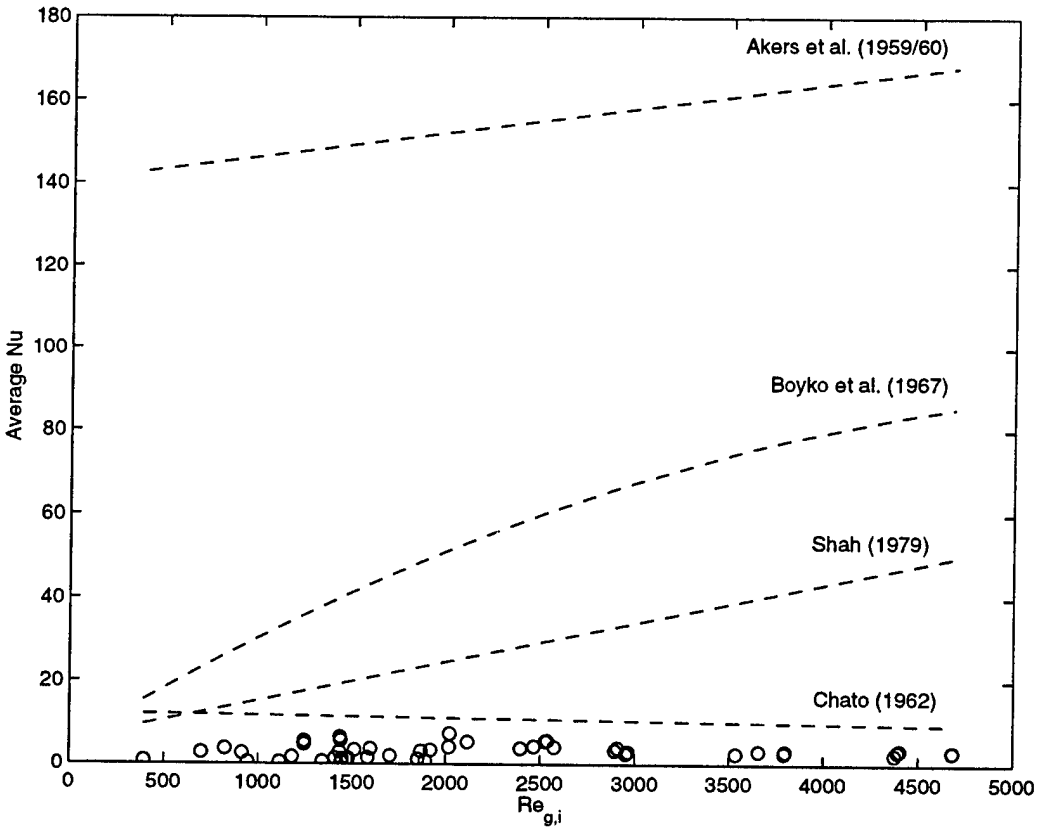

Figure 4.1. Comparison of Average Experimental Nusselt Number with Correlations in the Literature

The Nu data from the experiments are compared to the macroscale correlations in Figure 4.1. In this comparison, the Reynolds number of the inlet saturated vapor is selected as a common coordinate. It is seen that the current experimental data are much less than all the macroscale correlations. Chato's correlation appears to be the best of all the correlations in predicting the experimental data. Upon closer examination of the Chato correlation, revealed in Figure 4.2, the departure is still very apparent. The value of Nusselt number averaged over the overall range of the experimental Reynolds numbers is approximately 3.06. The Nusselt numbers of the chosen correlations for the current comparison from that of Chato, Shah, Boyko et al., and Akers et al. are approximately 3, 10, 20 and 50 times higher, respectively, than the averaged experimental Nusselt number (3.06).

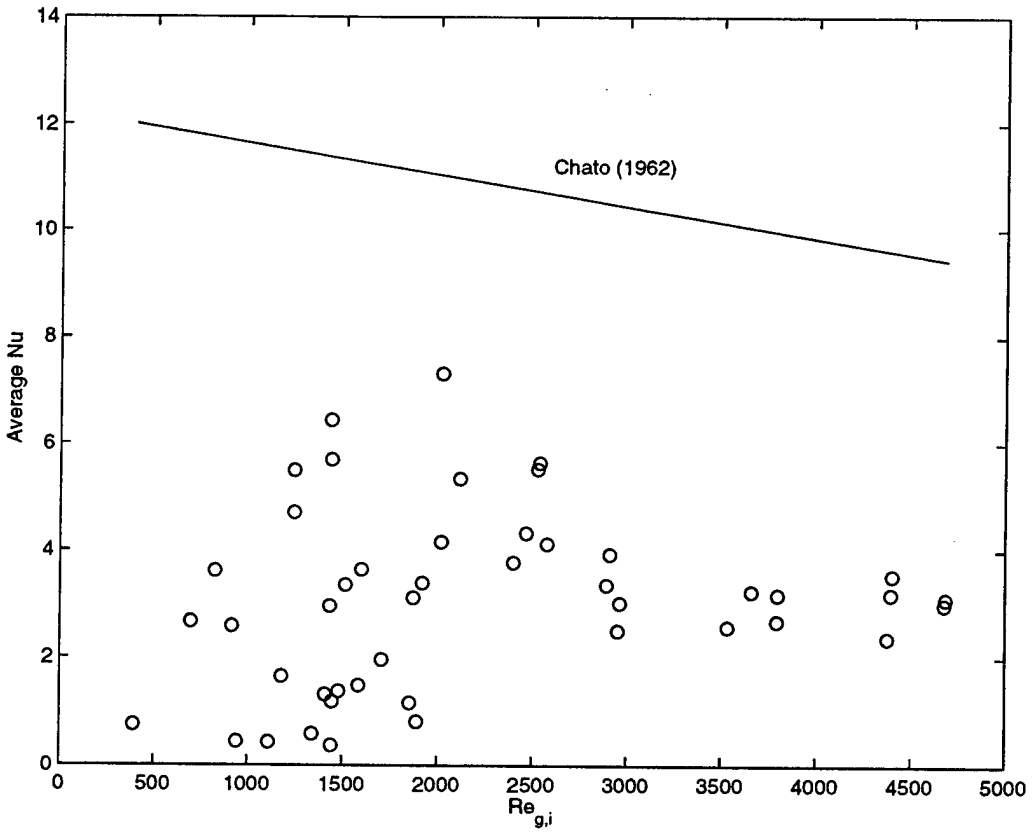

Figure 4.2. Comparison of Experimental Nusselt Numbers with Chato's Correlation

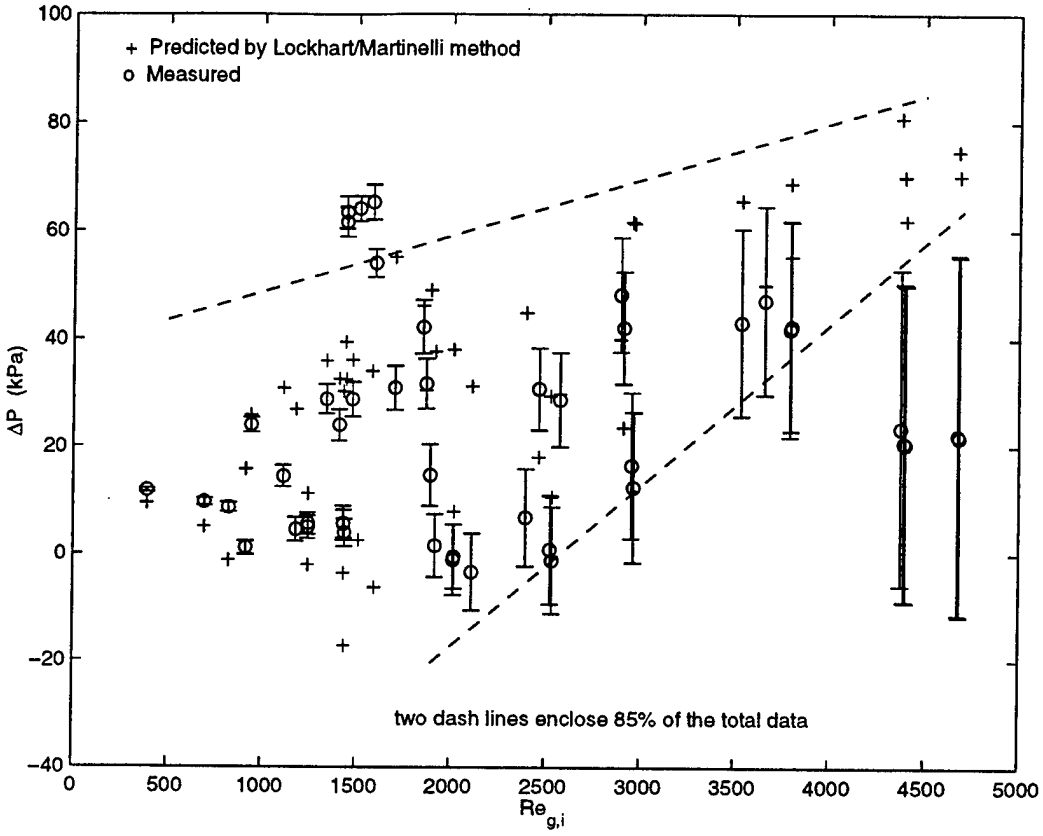

Figure 4.3. Comparison of Pressure Drops

4.3.2 Pressure Drop

A comparison of experimental pressure drop with that predicted by the Lockhart and Martinelli method [35] is shown in Figure 4.3. It is seen that the experimental pressure data are mostly located in the range of prediction, which account for about 85% of the total data.

4.4 Correlation of Experimental Nusselt Numbers

Conventional data correlating methods for film condensation in horizontal tubes have been attempted to correlate the current experimental Nusselt numbers, but they appear to not be applicable.

First, no obvious direct relationship between the average Nusselt numbers ($\overline{Nu}$) and Reynolds numbers ($Re_{g,i}$) is found, and then, the method used by Akers et al. [29, 30] is also attempted.

As described in Chapter 2, Akers et al. [29, 30] used four dimensionless parameters to correlate their data of the average Nusselt number for annular flow as shown in Eq. (2.6). When the film flow is laminar ($Re_f \leq 5,000$) and the Prandtl number is constant as is the case in the current experiment, four dimensionless parameters used by Akers et al. can be reduced to two. That is, the average Nusselt number has the the form of

$$\overline{Nu} = ARe_{g,eq}^{B}\Delta T^{*C},$$

where A, B, C are constants. Unfortunately, this method does not produce a good correlation in the current experiment.

One possible explanation for the above results is that the range of Reynolds number (approximately $500 \leq Re_{g,i} \leq 5,000$) in the current experiment is so narrow that no obvious trend can be observed, given the large data uncertainty. This can be the similar situation to that occurring in macroscale condensation experiments as discussed in Chapter 2.

The only obvious relationship found for the experimental Nusselt numbers that reasonably correlates the data takes the form of

$$Nu = 9.60\Delta x^{1.05}, \tag{4.1}$$

where Δx is the change of vapor quality from the inlet to outlet of the microtube. It is noted that this correlation is almost linear. Fig 4.4 depicts this correlation. It is seen that the experimental data are located in the range of -50% to $+75\%$ of the above correlation.

It was mentioned previously that all the correlations available in the literature and presented in Chapter 2, except that of Chato, include vapor quality as one of dimensionless variables for correlating Nusselt numbers (see Eq. (2.27)). Therefore, the correlation currently obtained for Nusselt numbers, Eq. (4.1), could be used as a correlation in the design of condensers. The sole dependence of Nusselt number on the change of vapor quality found in the current experiment simplifies its application in a design process. On the other hand, the very small range of parameters tested limits its general applicability.

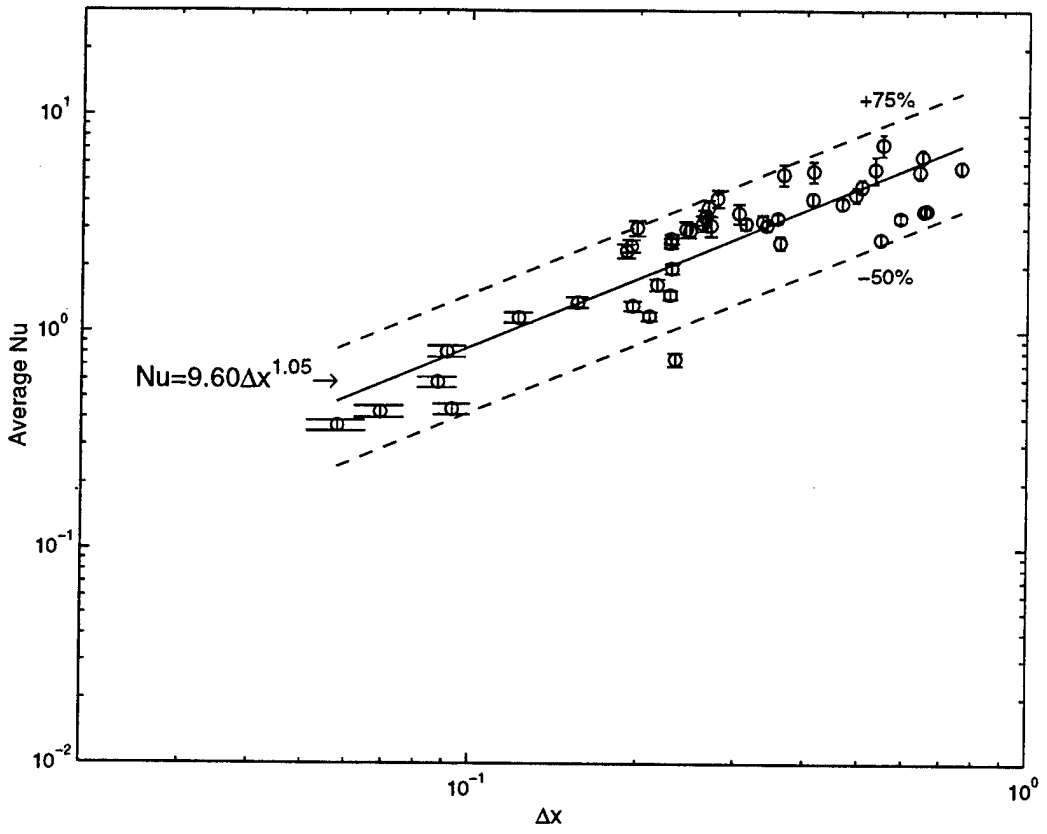

Figure 4.4. The Effect of Quality Change on Nusselt Number

4.5 Correlation of Dimensionless Temperature vs Reynolds Number

Experimental data reveal that dimensionless temperature can be related to Reynolds number of the inlet saturated vapor as

$$\Delta T^* = 2.17 \times 10^3 Re_{g,i}^{-0.509}. \tag{4.2}$$

Figure 4.5. shows this correlation. Experimental data are located in the range of -35% to $+70\%$ of the correlation.

As discussed previously, no dependence of $\overline{Nu}$ on $Re_{g,i}$ is observed in the experiment. Thus, the average condensing heat transfer coefficient ($\overline{h}$) may be assumed to be a constant in the range of $Re_{g,i}$ tested. On the other hand, it was observed in the experiment that the heat flux ($\dot{q}$) removed by the cooling water

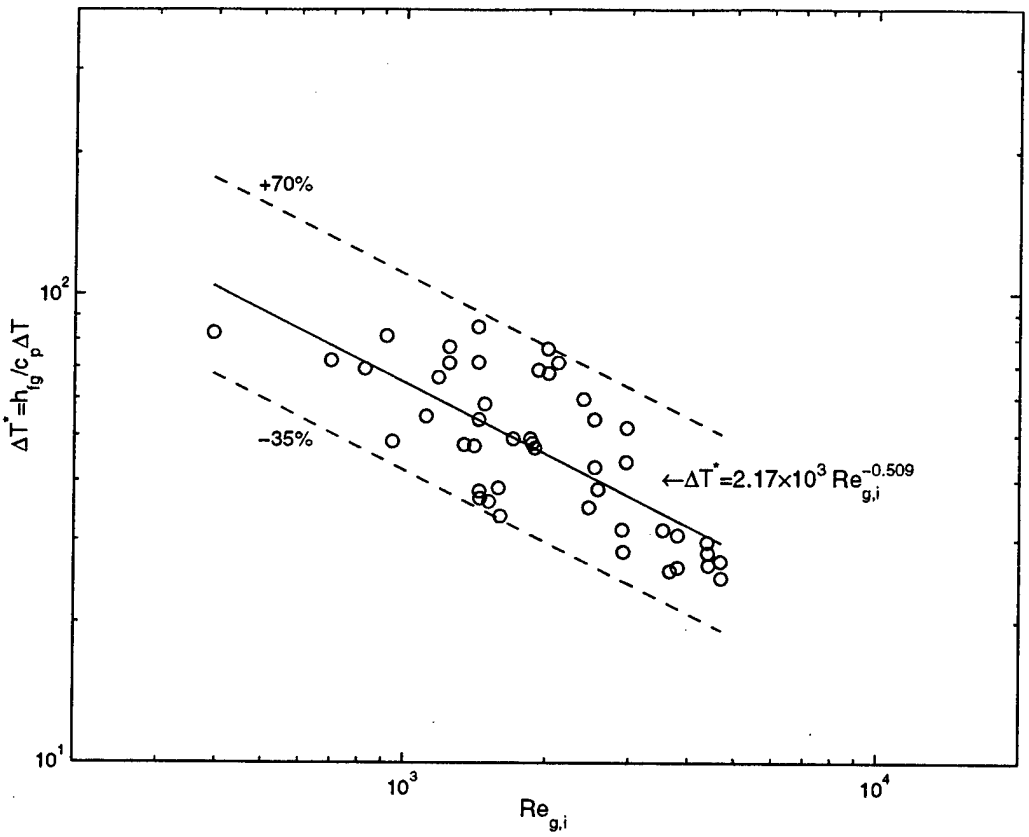

Figure 4.5. The Effect of Inlet Saturated Vapor Reynolds Number on Dimensionless Subcooled Temperature

was increasing with increasing $Re_{g,i}$ when other parameters were fixed. Therefore, based on the Newton's law of cooling

$$\dot{q} = \overline{h} \Delta T,$$

the subcooled temperature difference (ΔT) will increase with increasing $Re_{g,i}$. This corresponds to the trend indicated in Eq. (4.2) (note that $\Delta T^* \propto \Delta T^{-1}$).

4.6 Uncertainty

The uncertainties of two phase pressure drop and Nusselt number have been shown in Figure 4.3 and Figure 4.4, respectively. The detailed uncertainty analysis procedure is given in Appendix A. The following are the ranges of relative uncertainties for Nu, x_2, $Re_{g,i}$, and ΔP:

1. Uncertainty of $\overline{Nu} = \pm 4.6 \sim 14.1\%$
2. Uncertainty of $x_2 = \pm 0.4 \sim 14.9\%$
3. Uncertainty of $Re_{g,i} = \pm 8.3 \sim 9.6\%$
4. Uncertainty of $\Delta P = \pm 1.2 \sim 180\%$

4.7 Discussion

It has been seen that Nusselt numbers for the chosen correlations from macrotubes have approximately 3 to 50 times larger values than the current experimentally determined Nusselt numbers. These chosen correlations represent a wide range of film condensation from stratified flow to annular flow. As mentioned earlier in this chapter, from the map of flow pattern and the values of the experimental Nusselt numbers, the current experimental results should be in the spray flow regime in which Nusselt numbers should be even greater than those of annular flow. However, according to Chato's recommendation, the current experimental results would appear to be in the stratified flow regime. The experimental results do not agree with both flow types, in particular the spray flow results. The experimental Nusselt numbers are much smaller than the expected Nusselt numbers for spray flow (approximately 50 times smaller). Although Chato's correlation is found to be the best of all the correlations at predicting experimental data, the experimental data is still a factor of 3 less than the expected values. In addition, it is also found that the experimental Nusselt number does not show any dependence on Reynolds number (for the range of Re values considered) or vapor velocities, and only depends on the changes of vapor quality.

It has been mentioned previously that the narrow range of Reynolds numbers obtained in the experiment may be the main reason that an obvious trend of the $Nu-Re$ relationship was not observed. As for the dependence of Nu on the changes of vapor quality, the increase in Nu with the increase in Δx is due to the increased heat transfer associated with increased condensation. Thus, the remaining question to be answered is why the experimental Nusselt numbers are so small.

When estimating sizes of the droplets formed due to condensation, it is apparent that droplet sizes could be on the same order as the inside diameter of the microtube. Bonabian [42], Kataoka et al. [43], Mugele and Evans [44], and Wicks and Dukler [45] studied droplet size distribution in large-tube annular two-phase flow without phase change where droplet formation is mainly due to the droplet entrainment mechanism. Kataoka et al. [43] obtained the following equation to determine the average linear diameter of droplets D_{10}:

$$D_{10} = 0.0031 \frac{\sigma}{\rho_g u_g^2} Re_g^{2/3} \left(\frac{\rho_g}{\rho_f}\right)^{-1/3} \left(\frac{\mu_g}{\mu_f}\right)^{2/3}, \tag{4.3}$$

where σ is the surface tension, and Re_g is the vapor Reynolds number defined as

$$Re_g = \frac{\rho_g u_g d_i}{\mu_g}. \tag{4.4}$$

Although the mechanism of droplet formation in the current experiment is unclear, Eq. (4.3) may be applied to determine the order of magnitude of droplet sizes. Using Eq. (4.3), the droplet diameter distribution for the current experiment is calculated and then plotted in Figure 4.6, where the dash line represents the inside diameter of the microtube. In this calculation, quantities in Eq. (4.3) including the vapor velocity and all the fluid properties are based on average conditions between the inlet and outlet of the microtube. It is seen from Figure 4.6 that droplet diameters are at least on the same order as the inside diameter of the microtube. Thus, it seems reasonable that droplet size should be considered an important factor that affects the current experimental results.

Due to the large droplet sizes relative to the inside diameter of the microtube, the flow pattern in the current experiment should not be categorized as spray flow, annular flow, or stratified flow, all of which are based on macroscale concepts. The flow is more likely an intermittent flow in which the large liquid component fills the entire cross section of the microtube as shown in Figure 2.1. In the current case, the liquid component may be considered to be the result of droplet formation along the flow direction in the microtube. Figure 4.7 schematically illustrates an

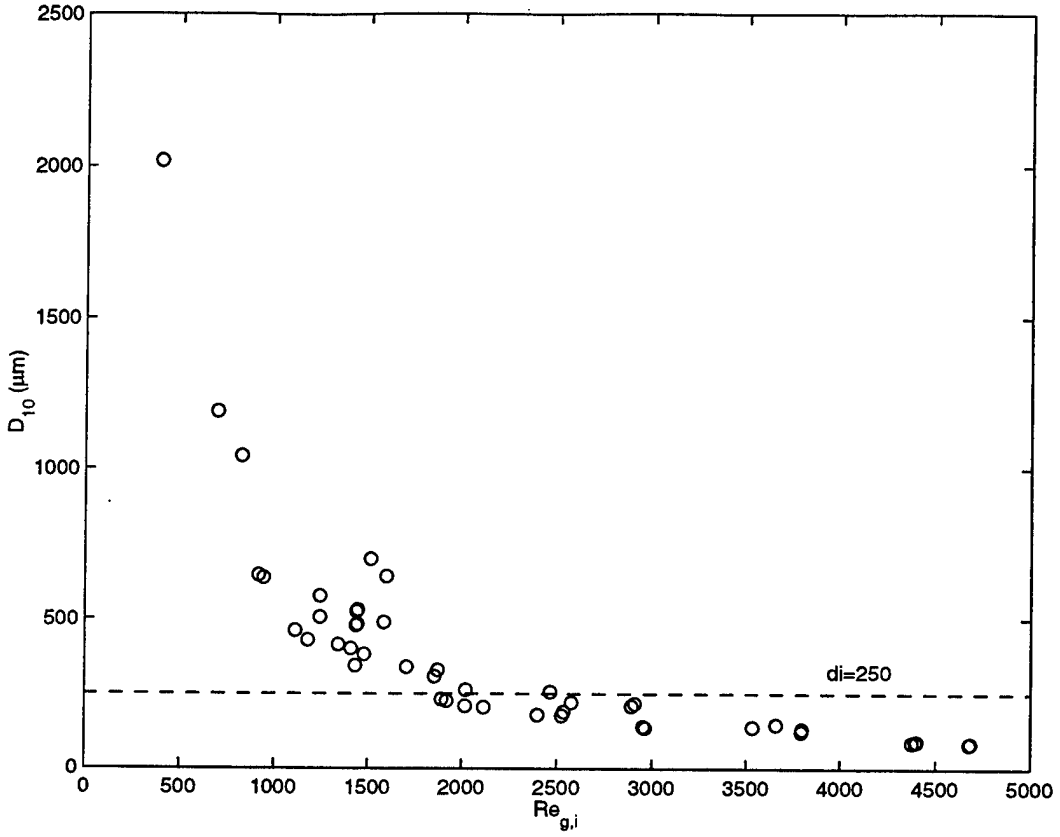

Figure 4.6. Droplet Size Distribution

expected flow pattern. With the alternating liquid and vapor regions, the surface tension force will become important in the current case.

The estimated shape of the liquid component in the microtube may look like that shown in Figure 4.7. The liquid region has a back concave surface and a front flat surface almost perpendicular to the flow direction. This is due to the result of forces acting in the liquid including the downstream pressure, upstream pressure, the frictional force, and the surface tension force. The contact angles due to the surface tension for the front surface and back surface are assumed to be 90^o and θ (where $\theta \neq 90^o$), respectively. This means that the surface tension force on the back surface would act solely against the pressure difference.

It was observed in the experiment that the condensate liquid erupted periodically from the end of the microtube into the atmosphere. This seems to support the flow pattern theory proposed above. A force balance in the streamwise direction

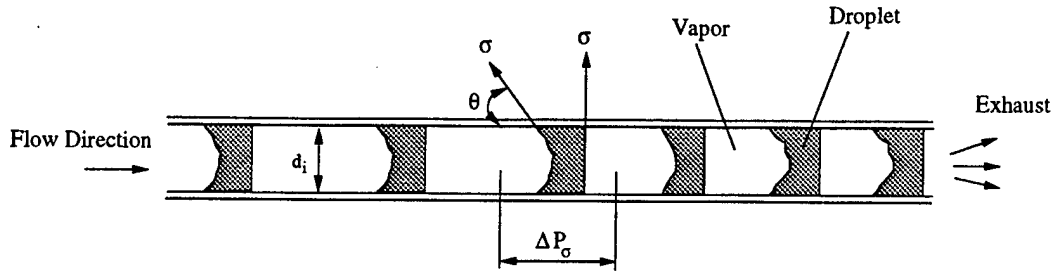

Figure 4.7. Condensation Flow Pattern Inside a Microtube

on each drop of liquid, neglecting frictional forces, gives

$$\Delta P_\sigma \frac{\pi d_i^2}{4} = \pi d_i \sigma \cos\theta. \tag{4.5}$$

Thus, the minimum pressure difference needed to overcome the surface tension force is

$$\Delta P_\sigma = \frac{4\sigma}{d_i} \cos\theta. \tag{4.6}$$

Evaluating the surface tension of saturated water at 100^oC and 1 atm and assuming a constant angle $\theta = 45^o$, the pressure difference will be

$$\Delta P_\sigma = \frac{4 \times 58.9 \times 10^{-3} N/m \cos 45^o}{250 \times 10^{-6} m} = 0.66 kPa. \tag{4.7}$$

That is, at least $0.5kPa$ pressure difference is needed to move each drop of condensate liquid in the microtube. Additional pressure difference will be needed to overcome both frictional pressure drop and the momentum change pressure drop as described in Chapter 2.

The "spitting" of fluid from the microtube outlet may be explained by the alternating liquid and vapor regions within the microtube. In addition, the approximate $1kPa$ pressure difference required to overcome the surface tension force and to push a liquid droplet of condensate liquid from the microtube may be unavailable at some times. The local pressure on the upstream side of the liquid region near the exit will have been reduced in overcoming the foregoing pressure requirements including those for frictional pressure drop, momentum change pressure drop, and

surface tension pressure drop. Thus, the liquid will cease to flow temporarily at the exit until the vapor pressure on the upstream side of the liquid region is increased by compression from the adjacent liquid region. When the last liquid region is ejected from the outlet, it will be replaced by the adjacent liquid region and the process will repeat. The result of this flow pattern and process at the exit is the intermittent "spitting" of liquid that was observed experimentally.

The condensation heat transfer coefficient with this kind of flow pattern will be smaller than that for spray flow, annular flow, or stratified flow since the contact area between the vapor and the cold tube wall will be greatly reduced by the large condensate drops. This is the most likely explanation for the small experimental Nusselt numbers.

It is apparent that the two-phase pressure drop inside microtubes should take into account the surface tension effect. As seen from Eq. (4.6), pressure drop due to surface tension is inversely proportional to the inside diameter of a microtube. Furthermore, it is noticed that Eq. (4.6) represents the pressure difference that is used to overcome only one drop of condensate liquid. For more than one drop of condensate liquid within the microtube, the total two-phase condensation pressure drop should be revised to be

$$\Delta P = \Delta P_f + \Delta P_m + N\Delta P_\sigma, \tag{4.8}$$

where N is the number of drops of condensate liquid. Note that the last term in Eq. (4.8) is only applicable in microtubes with liquid regions that completely fill the cross section. In the current experiment, the total pressure drop ranged from near zero to $65kPa$ with uncertainties from $\pm 1.2 \sim 180\%$. Given the level of experimental uncertainty and the lack of data regarding the number of condensate droplets in the tube, the actual experimental surface tension effect can not be ascertained.

4.8 Other Factors that may Affect Experimental Results

Two additional factors may have influenced the current experimental results. These effects are the result of the presence of noncondensible air and high velocity heating.

In the experiment, tap water was used as the condensing medium. Although it is unclear how much air is dissolved in the tap water, the noncondensible air will certainly influence the condensation heat transfer.

In a mixture of saturated steam and air, the partial pressure of the steam will be lower than the total pressure. The reduction in pressure of the steam will increase with increasing air content. Due to this reduction of pressure, the corresponding saturated temperature of the steam will be lowered, resulting in a smaller temperature difference between the steam and the cold wall. This is the reason that condensation heat transfer is degraded when noncondensible air is present. Stephan and Laesecke [46], and Sparrow et al. [47] investigated the forced convection condensation of steam from a mixture with air. Their studies showed that an approximately 10%, 20%, and 30% reduction in condensing heat fluxes occurred when the partial pressure of air accounted for 2%, 5%, and 10% of the total pressure of the mixture, respectively.

The current experimental Nusselt numbers are found to be 3 to 50 times lower than those obtained from macroscale results. Thus, noncondensible air should not be a critical factor in explaining the dramatical decrease in condensation heat transfer in the current experiment.

Referring to Table 4.1, the velocity of the inlet saturated vapor is up to $270 m/s$ in the current experiment. This high velocity may be one of factors that decreases the condensation heat transfer in the microtube compared to macroscale tubes.

In single-phase flow, the heating effect causes the addition of enthalpy to the fluid due to the conversion of high velocity kinetic energy of the fluid when the fluid is experiencing a deceleration process. The effect associated with this process includes the addition of heat, and an increase in temperature and pressure in the

fluid. The properties of the fluid will also change accordingly. The Nusselt number in single phase flow is related to the heat transfer and temperature difference as

$$\overline{Nu} \propto \frac{Q}{T_{wl} - T_f}.$$

Because both the amount of heat (Q) and the temperature of the fluid (T_f) in a high velocity process include the contribution of the high velocity heating, respectively, the Nusselt number which excludes the effect of the high velocity heating will essentially be smaller than that including the contribution.

However, in the condensation flow in a tube, the degree of reduction of the condensation heat transfer coefficient caused by the effect of the high velocity heating is difficult to be estimated. This is primarily due to the change of the vapor velocity along the flow. For instance, the vapor velocity will be zero when a complete condensation is reached, although there has been a high velocity of vapor at the inlet of the tube.

CHAPTER 5

CONCLUSIONS AND RECOMMENDATIONS

This thesis reports preliminary experimental results of forced convection condensation of steam inside a horizontal microtube. Conclusions and recommendations are given below.

5.1 Conclusions

The inside diameter of the tested microtube is the smallest so far seen in similar experiments. It was found that the average experimental Nusselt numbers of condensation (1) significantly deviate from those acquired in macrotubes, (2) do not depend on Reynolds numbers of inlet saturated vapor or inlet saturated vapor velocities, and (3) only show dependence on the changes of vapor quality across the microtube. The significant deviations observed from the previously reported macroscale results may be due to a different condensation mechanism caused by relatively large deoplet sizes compared to the inside diameter of the microtube tested. The two-phase pressure should include the contribution of surface tension. On the other hand, it is also noticed that the small number of data and other limitations in the current experiment have prevented further conclusions to be drawn. A large of number of future studies are needed.

5.2 Recommendations

In view of limitations involved in the current experiment, some suggestions for further studies are offered as follows.

1. Include a wider range of sizes of microtubes in order to investigate effects of geometries on condensation. This may include finding the sizes at which con-

densation Nusselt numbers or pressure drops start to deviate from macroscale results.

2. Test different kinds of fluid to study effects of fluid properties on condensation.

3. Increase the range of Reynolds numbers to better observe the expected Re effects.

4. Study effects of surface roughness on condensation.

5. Investigate effects of orientation of microtubes because correlations for annular flow condensation available in the literature are also applicable to non-horizontal macrotubes.

6. Improve experimental accuracy. This can be realized by reducing number of intermediate steps that are used to determine the average Nusselt numbers. For instance, using copper instead of stainless steel in the current experiment is expected to improve the accuracy of experimental average Nusselt numbers because the effects of thermal conduction in the microtube walls may be ignored due to the much higher thermal conductivity of copper than that of stainless steel. Additionally, the accuracy can be increased by directly measuring some quantities instead of making assumptions and simplifications for them. For instance, directly measuring the inlet vapor quality would improve the experimental accuracy.

7. Visualize the process of condensation to obtain a better understanding of the formation of condensate and the distribution of condensate or vapor in microtubes. To do so, using microchannels instead of microtubes may be a better scheme.

APPENDIX A

UNCERTAINTY ANALYSIS

For a result, F, which is a function of a set of variables $(x_1, x_2, \cdots, x_n)$, the absolute uncertainty of F is

$$dF = \sqrt{\sum_{i=1}^{n} \left(\frac{\partial F}{\partial x_i} \delta x_i \right)^2}.$$

This is the basic working equation for an uncertainty analysis. In this equation, $\frac{\partial F}{\partial x_i}$ is called the sensitivity coefficient which can indicate how sensitive the variation of the function, F, to the variation of the variable x_i will be, $\frac{\partial F}{\partial x_i}\delta x$ represents the contribution of the variable x_i to the total uncertainty (dF) of the function F, and δx_i is the uncertainty interval. The uncertainty interval, δx_i, may usually be set to be half the smallest scale division of the instrument. Relative uncertainty of F is defined as

$$\frac{dF}{F} \times 100\%.$$

Uncertainties of current experimental results are obtained using an uncertainty reduction computer program that is made based on the Moffat method [48]. The key point in this program is to find the sensitivity coefficients by using the central-difference definition of a partial derivative, that is,

$$\frac{\partial F}{\partial x_i} = \lim_{\varepsilon \to \infty} \frac{F(x_1, x_2, \cdots, x_i + \varepsilon, \cdots, x_n) - F(x_1, x_2, \cdots, x_i - \varepsilon, \cdots, x_n)}{2\varepsilon},$$

where the incremental variable, ε, may be set to a sufficiently small number to obtain accurate enough $\frac{\partial F}{\partial x_i}$.

In the uncertainty reduction program, $\varepsilon = 10^{-6} x_i$ for all the 15 variables which are used to determine Nusselt number (Nu), vapor quality (x_2) at the outlet of

the microtube, Reynolds number ($Re_{g,i}$) of inlet saturated vapor, and two-phase pressure drop (ΔP). The determination of measurement uncertainty intervals, δx_i, of the 15 variables are based on data provided by manufacturers of the instruments. These uncertainty intervals are listed in Table A.1.

The following is a typical set of uncertainty data calculated by using the above uncertainty reduction program:

Raw experimental data are

1. $d_i = 0.25mm$
2. $d_o = 0.79mm$
3. $L = 47.90mm$
4. $D = 4.93mm$
5. $T_{w,i} = 23.3°C$
6. $T_{w,o} = 52.5°C$
7. $T_{spht} = 123.2°C$
8. $T_{wl,o,1} = 86.3°C$
9. $T_{wl,o,2} = 90.8°C$

Table A.1. Uncertainty Intervals

No.	x_i	δx_i	No.	x_i	δx_i
1	δd_i	$0.02(mm)$	9	$\delta T_{wl,o,2}$	$0.1\%T_{wl,o,2} + 0.6(°C)$
2	δd_o	$0.02(mm)$	10	$\delta T_{wl,o,3}$	$0.1\%T_{wl,o,3} + 0.6(°C)$
3	δL	$0.02(mm)$	11	$\delta T_{wl,o,4}$	$0.1\%T_{wl,o,4} + 0.6(°C)$
4	δD	$0.02(mm)$	12	δP_o	$0.667(kPa)$
5	$\delta T_{w,i}$	$0.1\%T_{w,i} + 0.6(°C)$	13	δP_{spht}	$2.59(kPa)$
6	$\delta T_{w,o}$	$0.1\%T_{w,o} + 0.6(°C)$	14	δV_{cd}	$2\%V_{cd}(ml/min)$
7	δT_{spht}	$0.1\%T_{spht} + 0.6(°C)$	15	δV_w	$2\%V_{cd}(ml/min)$
8	$\delta T_{wl,o,1}$	$0.1\%T_{wl,o,1} + 0.6(°C)$			

10. $T_{wl,o,3} = 90.2°C$

11. $T_{wl,o,4} = 89.5°C$

12. $P_o = 84.779kPa$

13. $P_{spht} = 32.19kPa$

14. $V_{cd} = 0.3400ml/min$

15. $V_w = 1.7800ml/min$

The corresponding uncertainties for $Re_{g,i}$, x_2, $\overline{Nu}$, and ΔP are

1. $Re_{g,i} = 2395.6 \pm 210.7$

2. $x_2 = 0.7328 \pm 0.0114$

3. $\overline{Nu} = 3.7670 \pm 0.3061$

4. $\Delta P = 6.7592 \pm 9.0678kPa$

APPENDIX B

EXPERIMENTAL DATA

The following table includes 46 sets of experimental data:

No.	1	2	3	4	5	6	7	8
$T_{w,i}(°C)$	22.8	22.8	22.8	23.1	23.1	23.2	23.1	23.1
$T_{w,o}(°C)$	48.7	50.0	50.0	51.5	48.2	51.3	44.6	43.0
$T_{wl,o,1}(°C)$	85.5	84.2	84.2	84.8	82.6	84.1	84.8	83.1
$T_{wl,o,2}(°C)$	89.0	89.1	89.1	90.2	89.1	89.4	87.3	86.4
$T_{wl,o,3}(°C)$	88.9	88.2	88.2	88.1	88.0	89.4	88.0	86.5
$T_{wl,o,4}(°C)$	91.8	91.1	91.1	91.5	91.5	92.2	92.0	91.8
$T_{spht}(°C)$	118.3	117.2	115.3	114.6	116.9	115.2	117.7	116.7
$\dot{V}_{cd}(ml/min)$	0.098	0.116	0.166	0.175	0.175	0.270	0.296	0.283
$\dot{V}_{w}(ml/min)$	1.170	1.560	0.793	1.770	2.520	1.510	2.960	4.500
$P_o(kPa)$	84.78	84.70	84.71	84.70	84.72	84.73	84.77	84.54
$P_{spht}(kPa)$	11.57	11.16	11.16	11.33	11.54	18.46	16.62	15.96
No.	9	10	11	12	13	14	15	16
$T_{w,i}(°C)$	22.4	22.5	22.5	22.9	22.9	22.9	23.3	23.3
$T_{w,o}(°C)$	51.9	54.2	46.7	49.4	53.7	46.5	52.5	45.1
$T_{wl,o,1}(°C)$	88.1	84.7	80.9	88.0	83.7	79.8	86.3	81.8
$T_{wl,o,2}(°C)$	91.7	89.0	86.3	91.5	88.8	86.2	90.8	88.2
$T_{wl,o,3}(°C)$	91.1	89.0	87.3	91.4	89.4	86.7	90.2	88.1
$T_{wl,o,4}(°C)$	90.0	88.5	87.2	90.3	89.2	86.1	89.5	88.0
$T_{spht}(°C)$	130.7	130.4	129.3	116.0	117.5	113.0	118.2	116.7
$\dot{V}_{cd}(ml/min)$	0.234	0.223	0.234	0.202	0.202	0.202	0.340	0.356
$\dot{V}_{w}(ml/min)$	1.120	2.390	3.630	1.120	2.390	3.6300	1.780	3.790
$P_o(kPa)$	84.66	84.67	84.70	84.74	84.72	84.71	84.75	84.76
$P_{spht}(kPa)$	75.14	71.08	61.71	15.21	13.34	11.33	32.19	27.78

No.	17	18	19	20	21	22	23	24
$T_{w,i}(°C)$	23.1	22.6	22.5	22.5	22.9	22.9	22.9	23.1
$T_{w,o}(°C)$	33.3	45.2	46.2	52.1	50.1	53.4	51.9	50.1
$T_{wl,o,1}(°C)$	75.5	89.6	87.6	85.7	89.2	88.0	87.6	88.2
$T_{wl,o,2}(°C)$	86.8	91.0	90.1	90.6	88.1	85.7	86.3	85.2
$T_{wl,o,3}(°C)$	86.8	91.0	90.1	90.6	88.1	89.2	89.2	89.2
$T_{wl,o,4}(°C)$	87.2	88.6	85.8	89.3	89.2	89.0	88.4	89.1
$T_{spht}(°C)$	116.7	110.7	110.9	117.1	125.7	120.3	120.1	120.3
$V_{cd}(ml/min)$	0.356	0.056	0.128	0.283	0.193	0.202	0.270	0.135
$V_w(ml/min)$	10.400	0.336	1.120	1.550	0.420	0.793	0.570	0.321
$P_o(kPa)$	84.69	84.73	84.69	84.71	84.71	84.73	84.70	84.71
$P_{spht}(kPa)$	24.81	12.47	4.89	17.67	37.14	32.78	31.64	28.20
No.	25	26	27	28	29	30	31	32
$T_{w,i}(°C)$	23.1	22.2	22.4	22.3	22.5	22.6	21.6	21.9
$T_{w,o}(°C)$	48.7	46.6	50.9	49.1	54.6	53.6	54.2	47.2
$T_{wl,o,1}(°C)$	88.2	89.6	87.9	90.0	87.0	87.2	90.5	82.5
$T_{wl,o,2}(°C)$	87.8	90.0	88.5	91.5	88.0	89.2	91.0	85.3
$T_{wl,o,3}(°C)$	88.30	91.2	90.5	92.5	90.7	90.6	91.2	88.9
$T_{wl,o,4}(°C)$	88.4	90.0	89.3	92.3	90.7	90.	1 89.6	88.9
$T_{spht}(°C)$	112.1	122.7	125.1	121.9	118.8	122.0	126.0	125.4
$V_{cd}(ml/min)$	0.158	0.213	0.213	0.270	0.270	0.425	0.425	0.372
$V_w(ml/min)$	0.299	0.380	0.947	0.792	1.660	1.550	1.660	3.630
$P_o(kPa)$	84.72	84.73	84.73	84.75	84.75	84.76	84.75	84.76
$P_{spht}(kPa)$	20.49	72.44	70.00	57.20	45.53	54.48	51.06	53.78

No.	33	34	35	36	37	38	39	40
$T_{w,i}(°C)$	21.9	21.1	22.5	22.4	22.6	22.6	22.6	22.6
$T_{w,o}(°C)$	38.2	56.5	46.2	39.6	53.4	52.1	55.0	44.1
$T_{wl,o,1}(°C)$	78.9	87.2	80.0	79.7	87.7	90.8	83.9	78.5
$T_{wl,o,2}(°C)$	84.1	89.1	84.0	83.1	89.1	91.2	85.2	80.1
$T_{wl,o,3}(°C)$	87.8	91.0	88.2	87.9	90.7	91.3	88.3	85.8
$T_{wl,o,4}(°C)$	87.8	89.7	88.5	87.8	90.6	90.3	89.1	87.8
$T_{spht}(°C)$	123.1	136.9	133.0	129.7	125.0	123.8	130.4	128.1
$V_{cd}(ml/min)$	0.356	0.560	0.560	0.540	0.246	0.213	0.425	0.425
$V_w(ml/min)$	6.340	2.260	4.440	6.340	1.120	0.721	2.780	5.360
$P_o(kPa)$	84.77	84.77	84.76	84.77	84.77	84.77	84.77	84.77
$P_{spht}(kPa)$	52.49	98.39	96.33	96.14	43.22	38.54	78.95	71.60

No.	41	42	43	44	45	46		
$T_{w,i}(°C)$	22.8	22.8	22.6	22.6	22.6	22.8		
$T_{w,o}(°C)$	55.2	55.3	49.5	38.1	37.6	50.0		
$T_{wl,o,1}(°C)$	86.7	87.6	83.3	79.5	80.2	84.8		
$T_{wl,o,2}(°C)$	88.1	89.1	85.2	84.1	85.1	87.5		
$T_{wl,o,3}(°C)$	90.7	90.9	89.6	88.0	88.2	89.4		
$T_{wl,o,4}(°C)$	90.5	89.5	89.2	88.0	88.1	88.6		
$T_{spht}(°C)$	133.7	133.6	130.6	127.7	129.3	129.4		
$V_{cd}(ml/min)$	0.521	0.643	0.643	0.643	0.688	0.688		
$V_w(ml/min)$	2.260	2.260	3.630	7.360	7.360	3.630		
$P_o(kPa)$	84.76	84.77	84.76	84.78	84.79	84.78		
$P_{spht}(kPa)$	92.33	101.70	97.30	95.66	107.28	108.51		

REFERENCES

[1] Bailey, D.K., Ameel, T.A, Warrington, R.O, and Savoie, T.I, 1995, "Single Phase Forced Convection Heat Transfer in Microgeometries - A Review", 30th Intersociety Energy Conversion Engineering Conference, Orlando, Florida.

[2] Peng, X.F., and Wang, B.X., 1993, "Forced Convection and Flow Boiling Heat Transfer for Liquid Flowing through Microchannels", International J. of Heat and mass transfer, Vol.36, No.14, p. 3421-3427.

[3] Stanley, R.C., Ameel, T.A., and Warrington, R.O, 1996, "Convective Flow Boiling in Microgeometries: A Review and Applications", Convective Flow Boiling, Proceedings of the 1st International Conference on Convective Flow Boiling, Ed.John Chen.

[4] Ameel, T.A., Papautsky, I., Warrington, R.O, Wegeng, R.O., and Drost, M.K., 1998, "Miniature Technologies for Advanced Energy Conversion and Transfer Systems", 2nd Symposium on Advanced Energy Conversion Systems and Related Technologies, Nagoya, Japan, Dec., Vol.1, p. 172-179.

[5] Papautsky, I., Ameel, T.A., and Frazier, A.B., 1998, "Single-Phase Fluid Flow in Microchannels", 2nd Symposium on Advanced Energy Conversion Systems and Related technologies, Nagoya, Japan, Vol.1, Dec., p. 186-187.

[6] Choi, S.B., 1991, "Friction Factors and Heat Transfer in Microtubes", D.E Dissertation, College of Mechanical and Industrial Engineering, Louisiana Tech University.

[7] Choi, S.B., Barron, R.F., and Warrington, R.O, 1991, "Fluid Flow and Heat Transfer in Microtubes", Micromechanical Sensors, Actuators, and Systems, ASME, New York, NY, DSC-Vol.32, p. 509-519.

[8] Yu, D., Warrington, R.O, Barron, R.F., and Ameel, T.A., 1995, "An Experimental and Theoretical Investigation of Fluid Flow and Heat Transfer in Microtubes", 4th ASME/JSME Thermal Engineering Joint Conference, Maui, Hawaii, March.

[9] Ma, S.W., and Gerner, F.M., 1993, "Forced Convection Heat Transfer for Microstructures", J. of Heat Transfer, Vol.115, p. 872-880.

[10] Pfahler, J., Harley, J., Bau, H., and Zemel, J., 1991, "Gas and Liquid Flow in Small Channels", Micromechanical Sensors, Actuators, and Systems, ASME, DSC-Vol.32, p. 49-60.

[11] Tuckerman, D.B., 1984, Heat Transfer Microstructures for Integrated Circuits, Ph.D Dissertation, Department of Electrical Engineering, Stanford University.

[12] Phillips, R.J., 1987, Forced-Convection, Liquid-Cooled, Microchannels Heat Sinks, Master of Science Thesis, Department of Mechanical Engineering, Massachusetts Institute of Technology, Cambridge, Mass.

[13] Weisberg, A., Bau, H.H., Zemel, J., 1992, "Analysis of Microchannels for Integrated Circuits", International J. of Heat and Mass Transfer, Vol.35, No.10, p. 2465-2474.

[14] Yu, S.P. and Ameel, T.A., 1998, "An Air-Cooled Microchannel Heatsink with High Heat Flux and Low Pressure Drop", accepted in the Proceedings of the 33rd National Heat Transfer Conference, Albuquerque, New Mexico, 1999

[15] Van Oudheusden, B.W., 1992, "Silicon Thermal Flow Sensors", Sensors and Actuators, Vol.30, p. 5-26.

[16] Pong, K., Ho, C., Liu, J., and Tai, Y., 1994, "Non-Linear Pressure Distribution in Uniform Microchannels", Applications of Microfibrication to Fluid Mechanics, FED-Vol.197, p. 51-56.

[17] Gravesen, P., Branebjerg, J., and Jensen, O.S., 1993, "Microfluidics - A Review", J. of Micromechanics and Microengineering, Vol.3, p. 168-182.

[18] Benett, W.J., Freltas, B.L., CiarIo, D., Beach, R., Sutton, S., Emanuel, M., and Solarz, R., 1993, "Microchannel Cooled Heatsinks for High Average Power Laser Diode Arrays", Proceedings of the SPIE - The International Society for Optical Engineering, Vol.1865, p. 144-153.

[19] Koh, J.C.Y., and Colony, R., 1986, "Heat Transfer of Microstructures for Integrated Circuits", International Comm. of Heat and Mass Transfer, Vol.13, p. 1789-1798.

[20] Yu, S.P. and Xin, M.D., 1994, "Analysis and Experiment on Gas Convection Microchannel Heat Exchangers", Proceedings of the 10th International Heat Transfer Conference, Brighton, UK, Vol.4, p. 459-464.

[21] Zhukov, V.M., and Yarmak, I.L., 1990, "Transient Heat Transfer in Two-Phase Cryogenic Liquid Forced Flows Under Step Heat Flux in Narrow Channels", Cryogenics, Vol.30, p. 282-286.

[22] Bowers, M.B., and Mudawar, I.M., 1994, "High Flux Boiling Low Flow rate, Low Pressure Drop Mini-Channel and Micro-Channel Heat Sinks", International J. of Heat and Mass Transfer, Vol.37, No.2, p. 576-582.

[23] Suo, M., and Griffith, P., 1964, "Two-Phase Flow in Capillary Tubes", J. of Basic Engineering, September, p. 576-582.

[24] Stanley, R.C., 1997, Two-Phase Flow in Microchannels, Ph.D Dissertation, College of Engineering and Sciences, Louisiana Tech University.

[25] Stephan, K., 1992, Heat Transfer in Condensation and Boiling, Springer-Verlag Berlin Heidelberg.

[26] Nusselt, W., 1916, "Die Oberflachenkondensation des Wasserdampfes", VDI zeitschrift, Vol.60, p. 541-546, p. 569-575.

[27] Chen, S.L., and Ke, M.T., 1993, "Forced Convective Film Condensation Inside Vertical Tubes", International J. of Multiphase Flow, Vol.19, No.6, p. 1045-1060.

[28] Chato, J.C., 1962, "Laminar Condensation Inside Horizontal and Inclined Tubes", ASHRAE Journal, Vol.4, No.252.

[29] Akers, W.W., Deans, H.A., and Crosser, O.K., 1959, "Condensing Heat Transfer Within Horizontal Tubes", Chemical Engineering Progress Symposium Series, Vol.55, No.29, p. 171.

[30] Akers, W.W., and Rosson, H.F., 1960, "Condensation Inside A Horizontal Tube", Chemical Engineering Progress Symposium Series, Vol.56, No.30, p. 145-149.

[31] Soliman, M., Schuster, J.R., and Berenson, P.J., 1968, "A General Heat Transfer Correlation for Annular Flow Condensation", Transactions of the ASME, J. of Heat Transfer, p. 267-276.

[32] Boyko, L.D., and Kruzhilin, G.N., 1967, "Heat Transfer and Hydraulic Resistance During Condensation of Steam in a Horizontal Tube and in a Bundle of Tubes", International J. of Heat and mass Transfer, Vol.10, p. 361.

[33] Traviss, D.P., Baron, A.B., and Rohsenow, W.M., 1971, "Forced-Convection Condensation Inside Tubes", ASHRAE Contract RP63, MIT Report No.DSR7291-94, July, Cambridge, Mass.

[34] Shah, M.M., 1979, "A General Correlation for Heat Transfer During Film Condensation Inside Pipes", International J. of Heat and Mass Transfer, Vol.22, p. 547-555.

[35] Lockhart, R.W., and Martinelli, R.C., 1949, "Proposed Correlation of Data for Isothermal Two-Phase, Two-Component Flow in Pipes", Chemical Engineering Progress, Vol.45, No.1 p. 39-48.

[36] Rohsenow, W.M., and Hartnett, J.P., 1973, Condensation in Handbook of Heat Transfer, McGraw-Hill.

[37] Sernas, V.,Verma, V.C., and Fletcher, L.S., 1979, "Condensation of Steam Inside a Horizontal Tube", Condensation Heat Transfer, the 18th National Heat Transfer Conference, San Diego, California.

[38] Cengel, Y.A., and Boles, M.A., 1998, Thermodynamics, an Engineering Approach, 3rd Edition, WCB/McGraw-Hill.

[39] White, F.M., 1986, Fluid Mechanics, 2nd Edition, McGraw-Hill.

[40] Incropera, F.P., and DeWitt, D.P., 1996, Introduction to Heat Transfer, 3rd Edition, John Wiley and Sons.

[41] MicroGroup, Inc., 1996, Small Diameter Tubing Specialists, 7 Industrial Park Road, Medway, MA02053.

[42] Bonabian, S., 1990, "Internal Flow Analysis with a Predictive Model for Droplet Size Distribution", Ph.D Dissertation, Department of Mechanical Engineering, University of Utah.

[43] Kataoka, I., Ishii M., and Mishima, K., 1983, "Generation and Size Distribution of Droplet in Annular Two-Phase Flow", ASME J. of Fluids Engineering, p 230-238.

[44] Mugele, R.A., and Evans, H.D., 1951, "Droplet Size Distribution in Sprays", Industrial and Engineering Chemistry, Vol.43, No.5, p 1317-1324.

[45] Wicks III, M., and Dukler, A.E., 1966, "In Situ Measurements of Drop Size Distribution in Two-Phase Flow – A New Method for Electrically Conducting Liquids", 3rd Int'l Heat Transfer Conference, Chicago, p 39-49.

[46] Stephan, K., and Laesecke, A., 1980, "The Influence of Suction in Condensation of Mixed Vapor", Warme Stoffubergtrag, Vol.13, p. 115-123.

[47] Sparrow, E.M., Minkowycz, W.J., and Saddy, M., 1967, "Forced Convection Condensation in the Presence of Noncondensables and Interfacial Resistance", International J. of Heat and Mass Transfer, Vol.10, p. 1829-1845.

[48] Moffat, R.J., 1982, "Contribution to the Theory of Uncertainty Analysis for Single-Sample Experiment", ASME J. of Fluids Engineering, p. 40-56.